Astrophys Space Sci (2020) 365:88
https://doi.org/10.1007/s10509-020-03798-2

REVIEW ARTICLE

The 21 μm and 30 μm emission features in carbon-rich objects

Kevin Volk[1] · **G.C. Sloan**[1,2] · **Kathleen E. Kraemer**[3]

Received: 9 March 2020 / Accepted: 11 May 2020 / Published online: 25 May 2020

Abstract We review the observational properties and possible carriers of the 21 and 30 μm features seen in the spectra of evolved carbon-rich objects. The 30 μm feature is generally taken to be due to MgS, possibly in combination with other sulfides. It is commonly assumed that the sulfides coat grains of SiC or amorphous carbon, but it remains unclear if coated grains can produce the observed feature given the low relative abundance of sulfur and the optical constraints on the thickness of the coating and size of the grains. The lack of optical constants for MgS at wavelengths below 1 μm hampers attempts to model the dust shells of these objects. A small number of alternative carriers have been proposed, but these have not been investigated thoroughly. The situation for the 21 μm feature is more ambiguous. Many carriers have been proposed, but each has issues, and none have gained broad support. The feature only appears in carbon-rich objects which have evolved off of the asymptotic giant branch but have not yet become planetary nebulae. The spectral class of the central star is typically F or G. The transient nature of the 21 μm feature is an important clue to the nature of its carrier. It appears with a variety of other infrared emission features related to complex hydrocarbons, including aliphatic species and polycyclic aromatic hydrocarbons, but correlations with specific features have proven difficult to quantify.

Keywords AGB and post-AGB · Mass-loss · Carbon · Circumstellar matter

This article belongs to the Topical Collection: Unexplained Spectral Phenomena in the ISM. Guest Editor: Sun Kwok.

✉ K. Volk
volk@stsci.edu

[1] Space Telescope Science Institute, 3700 San Martin Drive, Baltimore, MD, 21218, USA

[2] Department of Physics and Astronomy, University of North Carolina, Chapel Hill, USA

[3] Boston College, Institute for Scientific Research, 140 Commonwealth Avenue, Chestnut Hill, MA 02467, USA

1 The 30 μm emission feature

The 30 μm feature is not as well studied as other commonly observed dust features in evolved stars, such as the silicate features at 10 and 18 μm or the SiC feature at 11.3 μm. Silicates and SiC can be detected spectroscopically in the N band centered at 10 μm,[1] but the 30 μm feature appears in a much less studied spectral region. In particular no all-sky set of spectra are available at 30 μm, because this spectral region is too difficult from the ground and has not been covered by surveys from space-based telescopes. Nor do we have any photometric indices that are reliable indicators of the feature, because commonly used photometric bands do not sample it. Spectroscopy of individual targets indicates that the feature occurs only during phases of high mass loss during the evolution of carbon stars (and a small fraction of S-type stars). This phase occurs late in a carbon star's evolution on the asymptotic giant branch (AGB). Due to the lack of any complete spectroscopic surveys of carbon stars that can detect the feature, we cannot estimate the frequency of the appearance of the 30 μm feature among carbon stars in general.

This review will discuss the general observational properties of the feature and then discuss the carrier. Most of the

[1] The term "N band" refers to the atmospheric window between about 8 and 13 μm, while "Q band" refers to the longer wavelength window between 16 and 24 μm. See for example Cox (2000), page 145.

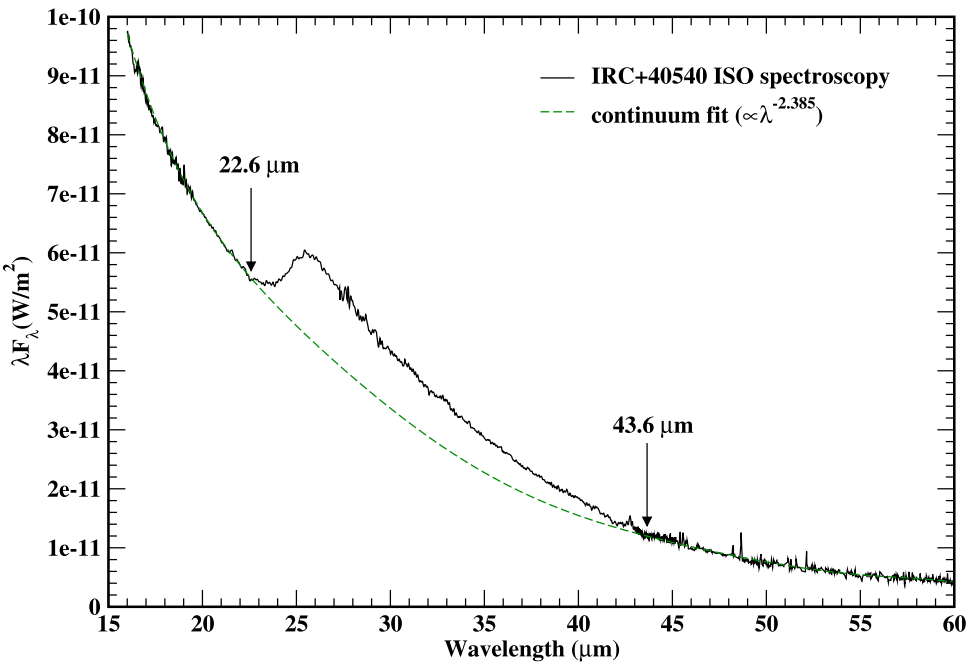

Fig. 1 An example of the 30 μm feature profile from the *ISO* spectroscopy of IRC+40°540. The continuum outside the feature has been fit with a power-law to approximate the spectral continuum under the feature, plotted as the green dashed curve. The range of wavelengths estimated for the feature are marked

work on the carrier of the feature in the literature has concentrated on MgS. The discussion here will therefore centre on whether MgS can produce the observed feature.

1.1 Observational properties

This feature was first identified by Forrest et al. (1981) in spectra from the Kuiper Airborne Observatory (KAO) of six bright carbon-rich objects in the 16 to 30 μm wavelength range. The broad feature, extending beyond the long-wavelength end of the spectra, was seen in four carbon stars with more optically thick dust shells and in two carbon-rich planetary nebulae (PNe). The feature was not seen in spectra of three other carbon stars which have dust shells of low optical depth. While the feature clearly peaked around 27 μm, it was simply dubbed the 30 μm feature.

Figure 1 shows an example of the feature profile as observed the carbon star IRC+40°540. The spectrum is plotted from 16 to 60 μm using data from the Short-Wavelength Spectrometer (SWS) and Long-Spectrometer (LWS) on the *Infrared Space Observatory* (*ISO*, Kessler et al. 1996). A power law in wavelength can fit the underlying continuum well. The feature peaks in the raw spectrum at 26.51 μm. Aside from the small tail at wavelengths between 22.6 and 24 μm, the feature shape is quite simple with a sharp rise to the peak and a long, rather uniform, decline back to the continuum.

The feature is very broad, and the *ISO* spectra indicate that it extends from ∼22.6 to ∼43.6 μm, almost a factor of two in wavelength. The silicate and SiC features observed in circumstellar dust shells are nowhere near this broad, so this feature is distinct in that respect; no companion features related to the 30 μm feature have been identified at other wavelengths. The feature does vary somewhat in shape and width from one source to another (Hony et al. 2002), but the feature always appears smooth without distinct sub-peaks in any individual spectrum. In the spectra from carbon stars with higher optical depths, the strongest 30 μm features peak at roughly 1.3 to 1.4 times the underlying continuum, similar to what Fig. 1 shows. For the objects that have left the AGB and are evolving to higher stellar temperatures, the feature becomes more prominent. The strongest 30 μm features in post-AGB objects peak at ∼2 times the estimated continuum level.

When one takes the ratio of the spectrum to the fitted continuum, the feature profile appears to be relatively flat across the shorter wavelength part of the profile before declining to the continuum at wavelengths beyond 37 μm, as Fig. 2 shows for sources IRC+20°236, IRC+40°540, and AFGL 2155. All three objects have strong 30 μm features and have both SWS and LWS spectroscopy from *ISO*, so the continuum can be fitted accurately. The shape of the continuum-divided feature varies from source to source. The wavelength where the initial rise occurs can shift by ∼0.5 μm. The relative shape across the feature appears different in IRC+20°236 compared to the other two sources. The S/N of the spectra limit our ability to further interpret the data. Unfortunately, spectroscopy from the *Spitzer Space Telescope* (hereafter *Spitzer*, Werner et al. 2004) ends at 37 μm, well before the long-wavelength end of the 30 μm feature. The partial coverage of the feature makes it difficult to define the underlying continuum.

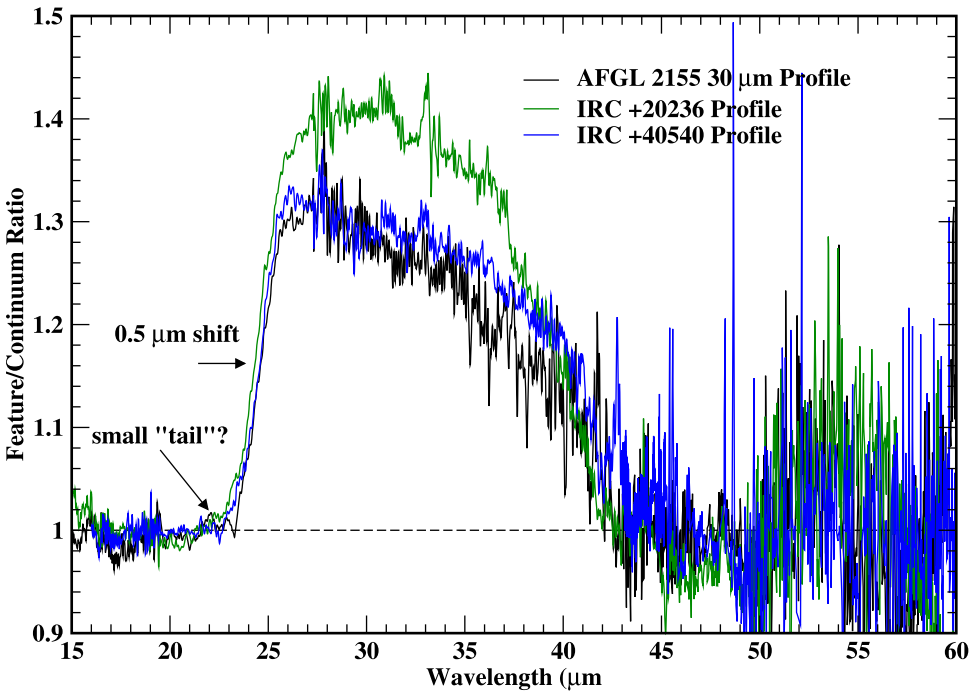

Fig. 2 Three examples of continuum-normalized 30 μm feature profile from the *ISO* spectroscopy. The three objects selected have fairly prominent features and have both SWS and LWS data which allow the continuum to be fit with a power law. There are some variations in the wavelength of the short wavelength edge of the feature. Variations in detailed shape of the profiles as also present

Even for carbon stars of similar spectral properties at the shorter wavelengths one can find examples of feature peaks from 26 to 27.5 μm. Figure 3 shows the *Spitzer* spectra of two objects studied by Leisenring et al. (2008). Although the spectra are a bit noisy, the peak wavelength of the 30 μm feature clearly differs in these two stars despite the general similarly of the spectra otherwise.

In spectra of carbon-rich PNe and post-AGB objects with spectral classes of B to G, the feature may peak at even longer wavelengths, out to 29.5 μm, although the peak in a few objects falls within the normal range for carbon stars. The cause of these shifts to longer wavelengths in post-AGB objects is not known. It might be purely a temperature effect in the dust grains (Hony et al. 2002), or it might indicate some type of change in the carrier of the feature. However, no individual spectrum shows evidence of multiple components. The early results from *ISO* suggested two sub-peaks in the feature at 26 and 33 μm (Volk et al. 2002). Later spectra of several of these objects from *Spitzer* showed that the feature is smooth and that the appearance of having two peaks was due to artifacts in the spectra from the *ISO* SWS band 3E data (Hrivnak et al. 2009).

ISO provided spectra of 63 carbon stars with the feature (Hony et al. 2002). *Spitzer* has provided the spectra of 187 objects with the feature (Gladkowski et al. 2019). Three of these stars were also observed by *ISO*, so the total number of objects where the feature is detected is 247. In some objects the feature is quite weak. Of note is that 12 S-type stars seem to have weak 30 μm features in their *Spitzer* spectra (Hony et al. 2009; Smolders et al. 2012). The original *ISO* sample from Hony et al. (2002) shows that the feature is absent in optically thin dust shells around carbon stars, and that it becomes more common as the optical depth increases, as was found from the small discovery sample. The larger *Spitzer* sample extends to the Magellanic Clouds and a few sources in other Local Group galaxies. It is not possible to extrapolate from the observed sample to estimate the total populations of 30 μm objects in the different systems, because the samples are selected for spectroscopy for a wide variety of reasons leading to a biased and heterogeneous sub-sample of objects with spectroscopy. Hony et al. (2002) examined 63 detections of the feature and 12 non-detections from a mix of *ISO* programs. The sample studied by Gladkowski et al. (2019) was assembled by looking at all *Spitzer* IRS programs that observed carbon-rich objects or S-type stars, but the non-detections were not tallied when the sample was assembled. The actual fraction of all Galactic carbon-rich AGB and post-AGB objects that have the feature should be much smaller than the Hony et al. (2002) numbers indicate, as carbon stars with low mass-loss rates are more common than those with high mass-loss rates, and such stars are less likely to have been selected for mid-infrared spectroscopy.

One could argue that the sample of post-AGB objects is less biased. The post-AGB objects discovered by the *Infrared Astronomical Satellite* (*IRAS*) are from a uniform all-sky survey. Because the number of candidate post-AGB objects is relatively small, a significant fraction of the sample have been subsequently observed by *ISO* or *Spitzer*. However, unknown biases must remain in the samples, because the post-AGB objects discovered solely by optical spec-

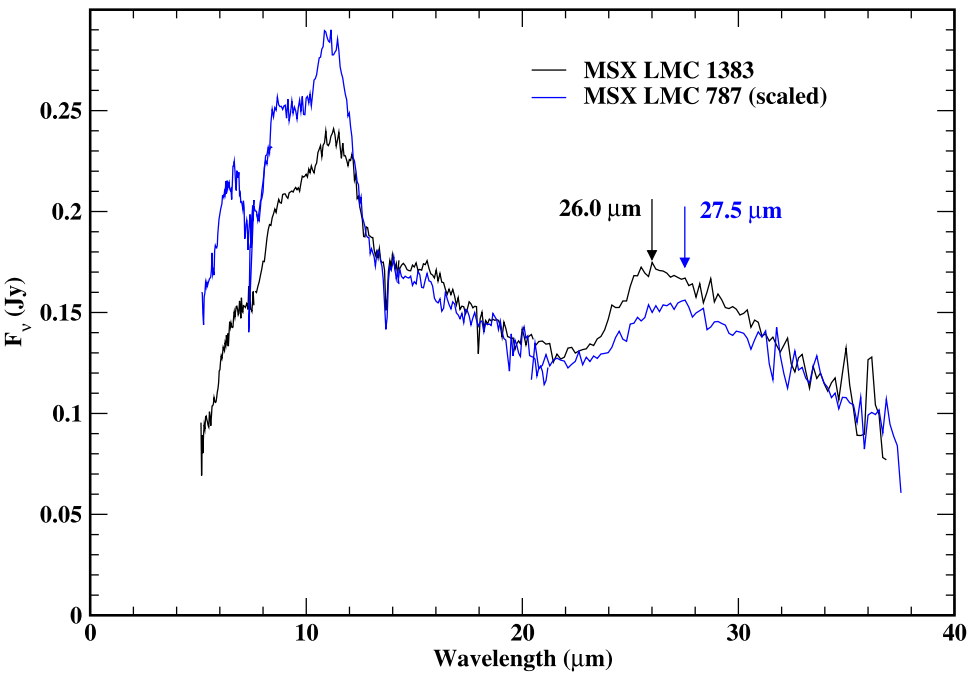

Fig. 3 Comparison of two *Spitzer*/IRS spectra of carbon stars in the LMC, from Leisenring et al. (2008). The spectrum of MSX LMC 787 has been scaled up to match the spectrum of MSX LMC 1383 at 16 μm. It appears that the peak of the 30 μm feature is shifted to ∼27.5 μm in the spectrum of MSX LMC 787 whereas the peak is at ∼26.0 μm in the spectrum of MSX LMC 1383

troscopy differ significantly from the *IRAS* objects. The optically selected post-AGB candidates, for example the stars discussed by Giridhar and Ferro (2005) and Bond et al. (2016), tend to have spectral classes of F or earlier, show little or no infrared excess, and are usually at higher galactic latitude than the *IRAS*-selected candidates.

A study of the *Spitzer* spectra of 25 Magellanic PNe by Bernard-Salas et al. (2009) showed that of the 17 objects that have infrared emission features commonly associated with polycyclic aromatic hydrocarbons, and hence are carbon-rich, 12 have the 30 μm feature. This suggests that a large fraction of carbon stars develop the feature sometime on the AGB, but probably only late in that phase of their evolution.

As discussed by Lagadec et al. (2012) and Gladkowski et al. (2019), the 30 μm feature weakens in more metal-poor stars. It is very weak in carbon stars in the thick disk and halo of the Galaxy (Lagadec et al. 2012). It is less common for carbon stars in the Large Magellanic Cloud (LMC) than for similar stars in the Galaxy (Sloan et al. 2006; Leisenring et al. 2008), and it is rare for carbon stars in the Small Magellanic Cloud (SMC). *Spitzer* spectroscopy of Magellanic carbon stars also revealed a number of highly obscured carbon stars that entirely lack the 30 μm feature (Gruendl et al. 2008), which has not been observed in Galactic carbon stars of similar high optical depth, as judged from the J−K or L−M colour for example. In Galactic carbon stars, one sees the 30 μm feature in stars with [6]−[9] colours from 0 to 1.7 magnitudes. In the LMC, the feature is only seen for [6]−[9] colours above ∼0.75 magnitudes, indicating that the feature appears at higher optical depths in LMC objects compared to objects in the Galaxy.

The 30 μm feature does not appear in the interstellar extinction curve. It also does not appear in the spectra of R CrB stars, even though these stars are carbon-rich post-AGB objects that can produce dust. The former indicates that the carrier does not survive long in the general interstellar medium (ISM) or is in general too rare to affect the extinction curve. That the R CrB stars do not produce the 30 μm feature presumably indicates that the carrier cannot form in environments which are hydrogen deficient.

1.2 Proposed carriers

1.2.1 MgS and related sulfur compounds

Soon after the discovery of the 30 μm feature, Nuth et al. (1985) and Goebel and Moseley (1985) proposed the MgS to be the carrier, with smaller contributions possible from CaS, and FeS_2. Almost all of the subsequent discussion in the literature has concentrated on MgS as the carrier. While MgS and several similar sulfur compounds do have broad features around 30 μm that are a reasonable match to the observed feature (see Messenger et al. 2013), it is difficult to confirm them as the carrier. The main issue in making radiative transfer models with MgS or similar dust species is that we only have measured optical constants at wavelengths longer than ∼1 μm, which misses much of the wavelength range where the dust is heated. For this reason only approximate MgS dust models can be made, for example assuming a single temperature for the grains in the shell independent of radius. Different investigators have tackled this issue in different ways (see Omont et al. 1995; Szczerba et al. 1999;

Hony et al. 2002, 2003; Zhukovska and Gail 2008; Lagadec et al. 2012). Within the limitations of these models, one can produce reasonable matches to the observed features either using pure MgS grains or assuming that MgS forms as a coating on the other dust grains observed in carbon stars.

The peak of the emission features from CaS, MgS, and FeS_2 grains covers a wavelength range of ∼2 μm, which could explain the observed variation in the position of the 30 μm feature in different objects. Changing the grain shape from spherical to ellipsoidal can also shift the peak of the features (e.g. the model for IC 418 by Gómez-Llanos et al. 2018).

Zhukovska and Gail (2008) studied the condensation of MgS into grains and concluded that direct condensation of MgS into grains is inefficient and that it is much more likely that MgS condenses onto pre-existing core grains, for which SiC was considered the best candidate. The condensation of MgS was found to only happen at gas temperatures below 600 K, so if one assumes the formation of SiC or carbonaceous dust at temperatures above 1000 K, then MgS cannot coat pre-existing grains in the inner dust shells around carbon stars. The efficiency of MgS coatings was still relatively low, on the order of 10% condensation onto grains of typical radius 0.1 μm, but the condensation would be more efficient with larger base grains. Zhukovska & Gail predicted that the MgS coating had to be thicker than about 0.08 μm to avoid having a double-peaked opacity function. They also found that MgS or CaS will condense much more efficiently onto SiC grains than onto carbonaceous grains due to the lattice structure of SiC grains. For more metal-poor stars, the amount of SiC that can form will be limited by the Si abundance irrespective of the total C overabundance, and one may then expect that carbon grains form preferentially over SiC grains at low metallicities. This may explain the lower incidence of 30 μm features in more metal-poor systems such as in the SMC. See the discussion by Sloan et al. (2006) concerning the dependence of the 30 μm feature on overall metallicity.

The known pre-solar SiC and carbonaceous graphite grains show no sign of an MgS coating or of MgS inclusions. However, a meteoritic pre-solar FeS inclusion has been detected within a pre-solar graphite grain (Haenecour et al. 2016). Hence some sulfur-bearing grains must exist in the ISM, even if we do not see direct evidence of them in the interstellar extinction curve. On the other hand, having a small FeS grain as an inclusion within an AGB graphite grain runs somewhat contrary to the simple formation scenarios where the carbon should condense well before FeS in a stellar outflow. This may indicate that the grain formation process is more complex than is generally assumed.

Many papers dealing with the dust shells of carbon stars assume an ISM-like size distribution dominated by very small grains. If one needs high efficiency in the MgS condensation, typical grain sizes rather larger than 0.1 μm would seem to be required based on the results from Zhukovska and Gail (2008), which is not consistent with the typically assumed size distribution. However, this has generally not been considered in dust shell models of these carbon stars.

1.2.2 Abundance problems with the MgS hypothesis

Omont et al. (1995) started a long-unresolved debate about whether the available abundance of sulfur in these stars is sufficient to produce the 30 μm feature. The main problem is that in many post-AGB stars with this feature, it carries a significant fraction of the total luminosity in the spectrum (30% or more). Omont et al. estimated that a sulfur abundance of about 0.5 solar was needed to produce sufficient MgS to carry this much energy in the spectrum, assuming 100% efficiency in producing MgS grains. However, many of the post-AGB stars with the feature are known to be of lower than solar metallicity, which poses a quandary. The measurements of SiS abundances in carbon stars and the predictions of chemical models both suggest that this much MgS cannot be produced in most carbon stars (e.g., Decin et al. 2010; Danilovich et al. 2018). Nor does one expect 100% efficiency in MgS grain production.

This issue has been pursued by others. For example, Zhang et al. (2009) found that the measured sulfur abundance in one object (HD 56126 = IRAS 07134+1005) is less than 20% of the amount required to explain the observed feature, based on rather general considerations of the dust emission and absorption efficiency. One caveat is that the optical constants for MgS are not known at short wavelengths, as noted above, and hence assumptions had to be made about them at ultraviolet and optical wavelengths. While the assumptions made seem quite reasonable and are conservative, they still mean that the conclusion is not definitive. On the other hand Hony et al. (2003) found that they could fit the *ISO* spectrum of this object with several dust components including MgS and that only 25% of the S needed to form MgS to explain the 30 μm feature. This rather drastic disagreement illustrates the difficulty of drawing conclusions given the current incomplete knowledge of the detailed physical properties of MgS grains.

The study of Magellanic PNe by Bernard-Salas et al. (2009) is one of the few cases where an independent sulfur abundance can be compared with the strength of the 30 μm feature. While their *Spitzer* spectra do not cover the full extent of the 30 μm feature, they were still able to conclude that the nebular S abundance does not correlate with the strength of the feature. In general one expects S depletion onto grains when the 30 μm feature is present if MgS or other sulfides are the carrier. The lack of S depletion in some of the PNe with the feature casts doubt on MgS as its carrier.

Lombaert et al. (2012) studied the 30 μm feature in the highly obscured carbon star LL Peg (more commonly

known as RAFGL 3068) and concluded that with coated grains, enough MgS is available to explain the observed feature, provided the metallicity of the star is close to solar. We will refer to such carbon stars with very optically thick dust shells as "extreme carbon stars" to indicate that they are likely to be close to the end of their lives on the AGB, and hence the most likely progenitors of the carbon-rich post-AGB objects and PNe. Their conclusion about the abundance depends somewhat on the assumption that the emitting dust grains all have the same temperature and that the observed emission arises entirely from the outer parts of the dust shell where the heating is due to infrared emission from deeper in the shell. These assumptions require further testing, and while they may be suitable for a carbon star embedded in a highly opaque dust shell, they are certainly not suitable for cases where the optical depth is small, whether in carbon stars with lower mass-loss rates or in post-AGB objects such as HD 56126. One also needs to consider that a large fraction of the Galactic carbon stars with abundance determinations have somewhat less than solar metallicities (e.g., Gonneau et al. 2017; Abia et al. 2019).

Many of the carbon-rich post-AGB objects have abundance determinations (although these may not include an explicit S abundance measurement), with values typically lower than solar by a factor of 3 or more. None of these objects have close to solar metallicity. Extrapolation of the optical depths back to the end of the AGB phase suggests that objects such as IRAS 22272+5435 and IRAS 06530−0213 were extreme carbon stars similar to RAFGL 3068 in the recent past. Given these uncertainties, the conclusion of Lombaert et al. (2012) that MgS grains fit the observed spectrum of RAFGL 3068 well without any abundance issues needs to be treated with caution. This type of analysis should be carried out for other 30 μm sources, including ones with less extreme dust shells. This approach would be especially important for stars with independent abundance information, either from the stellar spectrum or from molecular lines, to compare with the amount of S needed to produce MgS grains and match the observed strength of the 30 μm feature.

1.3 Resolved imaging and dust sizes

Starting with Meixner et al. (1997), several investigators have resolved thermal emission from the dust shells of a number of carbon-rich post-AGB objects with the 21 μm and 30 μm features (e.g., Lagadec et al. 2011). Where ground-based imaging has been obtained in both the N and Q bands, no significant differences have been found in the image structure at wavelengths around 10 μm and in filters that include the 21 μm feature and the blue side of the 30 μm feature (Kwok et al. 2002). This similarity suggests that the carriers of the long-wavelength features are well mixed with the carrier(s) of the continuum and the other infrared emission features seen in the N band for these objects.

The only cases known to the authors where such imaging has been obtained for the main part of the 30 μm feature are NGC 7027 and R Scl, observed with FORCAST on the *Stratospheric Observatory for Infrared Astronomy* (SOFIA) (Lau et al. 2016; Hankins et al. 2018, respectively). In NGC 7027, hotter dust within the ionized region dominates the emission at all wavelengths out to 37 μm, and no separation of the carrier of the 30 μm feature from the rest of the dust is apparent within the nebula. It is an interesting question how long MgS grains or coatings can survive within the harsh environment of the ionized region of NGC 7027. The dust emission is modelled as predominantly from fairly large grains (radius 1.5 μm) with a small fraction of much smaller grains (radius 0.0012 μm) that are presumed to be the result of breakdown of the large grains. The 30 μm feature in NGC 7027 presumably arises from the large grain component.

For R Scl the dust shell has a large angular radius (∼20″), and is assumed to have been produced by a thermal pulse that took place about 1900 years ago (Maercker et al. 2012). The available *ISO* SWS spectra of the source taken at different times are not very consistent, and the 30 μm feature is relatively weak. Hankins et al. (2018) modelled the dust shell with 86% amorphous carbon, 10% SiC, and 4% MgS by mass. They used a radiative transfer code and assumed two components: a hotter dust component representing on-going mass loss from the star, and a more massive, cooler dust component representing the shell from the thermal pulse. However, they did not describe how they handled the lack of optical constants for MgS dust grains at shorter wavelengths in their models. Hankins et al. (2018) conclude that the available observations do not place strong constraints on the MgS properties.

1.3.1 Combined image and spectral fitting

In cases where a dust shell is resolved in mid-infrared imaging and the spectral energy distribution (SED) allows a clear separation of the stellar and dust emission components it is possible to estimate the grain size by fitting the SED and the imaged size of the dust shell simultaneously. The physical basis is that when heated by a star the radius at which the dust grains have a specific temperature changes with the grain size. Smaller dust grains are less efficient radiators and more efficient absorbers of the stellar radiation than larger dust grains of the same composition. As a result, at a given distance from the star the smaller grains will be hotter than the larger grains. For an example of this effect in the interstellar context, see Fig. 3 of Li and Draine (2001). Conversely, the distance from the star for which the grains have a specific temperature will be greater for the smaller dust grains than for larger dust grains. For a given input stellar spectrum, grains below a limiting radius will have the

same temperature at a given distance because the differences in the grain cross-sections only appear at very short wavelengths where little or no stellar radiation is emitted. For post-AGB objects where the SED provides a firm limit on the maximum dust temperature in the shell, if one also has resolved imaging of the thermal dust emission, then one can estimate the grain size from the angular size of the emitting region. For a given assumed dust composition one can obtain robust estimates of the dust grain sizes in different objects.

However, this analysis cannot be applied to MgS because of the lack of optical constants at short wavelengths. It would be of considerable interest to have those constants and therefore be able to explicitly model whether a coated SiC grain or coated amorphous carbon grain can produce models which match both the SEDs and surface-brightness images. In the absence of MgS optical constants, models based on the optical constants for amorphous carbon are a way to estimate the grain sizes in different objects.

In the model by Hankins et al. (2018), as in many other such models, the dust grains were assumed to follow the usual ISM size distribution, and it is stated that this assumption does not strongly affect the modelling. For carbon stars in general we do not have resolved images at the scale of the inner dust-shell radius, hence one can assume an inner dust-shell temperature and use this to estimate the inner dust-shell radius without any constraints. In such cases, the size distribution may not affect the results much. Thus, attempting to apply the image and SED fitting is much easier in post-AGB objects where one has direct constraints on the inner dust-shell radius and temperature independently.

The use of averaged dust cross-sections to approximate a size distribution is in principle unphysical unless the grains are all interacting strongly enough to come to a common temperature at each radius. Such averaging of the coefficients works well in high optical depth cases but is less accurate for low optical depth dust shells. While the use of averaged cross-sections was required in the past the increase in available computer resources allows explicit modelling of dust size distributions with many independent grain sizes, which produces a more accurate result. It is hoped that this type of modelling will become more common in the future, especially in cases where the inner radius is directly constrained by the observations.

Results of the combined image and SED fitting using the BE type amorphous carbon grain cross-sections from Rouleau and Martin (1991) have been obtained for five objects by Volk (unpublished): IRAS 07134+1005, IRAS 23304+6147, IRAS 22272+5435, IRAS 19500−1709, and IRAS 14325−6428. Figure 4 shows examples of the model images for fitting IRAS 14325−6428 with different dust radii, along with a de-convolved Q-band image (22.1 μm) of the object obtained at the Gemini South telescope with the T-ReCS instrument. The models with small dust grains all predict larger angular sizes than what is observed, and the best match is found for grains of radius 2.0 μm. Larger grains produce models that are smaller in angular size, and the model surface brightness at 22.1 μm becomes significantly larger than the observed value.

IRAS 14325−6428 was selected for modelling because it has an unusually strong 30 μm feature. Figure 5 shows the model which best fits the SED of IRAS 14325−6428 with the dust grains mostly being of 2 μm radius, plus a smaller population of dust grains having radii from 0.3 to 1.0 μm with a power law number distribution of index −2. The maximum temperature of the dust grains is strongly constrained by the requirement that the model does not exceed the observed spectrum at any wavelength, subject to the accuracy of the observations. As the spectrum is on the short-wavelength side of the peak for the whole wavelength range from 8 to 18 μm the emission depends exponentially on the temperature, so the small uncertainties in the spectrum produce much smaller uncertainties in the maximum dust temperature. The smaller grains serve to produce a small amount of emission at wavelengths less than 10 μm, well below the SED peak, where the spectrum is not well fit by the primary population of 2 μm grains. In this model the grain-size distribution was approximated by 101 discrete grain radii, up to 2.0 μm. The models solve for all the dust grain temperatures independently as a function of radius and produce the combined spectrum. For the combined model the temperature of the 2.0 μm grains at the inner dust shell radius is 112 K, while for the smallest grains in the power-law component the temperature is 205 K.

Four other post-AGB objects with good ground-based imaging were modelled similarly, except that the models were fitted to observations in the N band. Table 1 summarizes the results. The surprise here was that a range of dust sizes was required to match the observed sky radii of the different objects. The fitting allows for ISM extinction and the intrinsic extinction, fits the SED for each grain radius, and then compares the predicted angular radius with the observed angular size to deduce the best-fit grain size. The models are limited to the extent that they assume a spherically symmetric dust shell, but those cases where the mid-infrared emission is optically thin should not produce large perturbations in the results. Some models were also made for the amorphous cross-sections from Zubko et al. (1996), and for the ACAR and AC2 sample types this did not produce much change in the derived grain size.

1.3.2 Implication for the MgS model

The grain-size results are of particular interest for the coated grain models that are used for the 30 μm feature. As noted above in the calculations of Zhukovska and Gail (2008), one needs an MgS coating of thickness about 0.08 μm for the

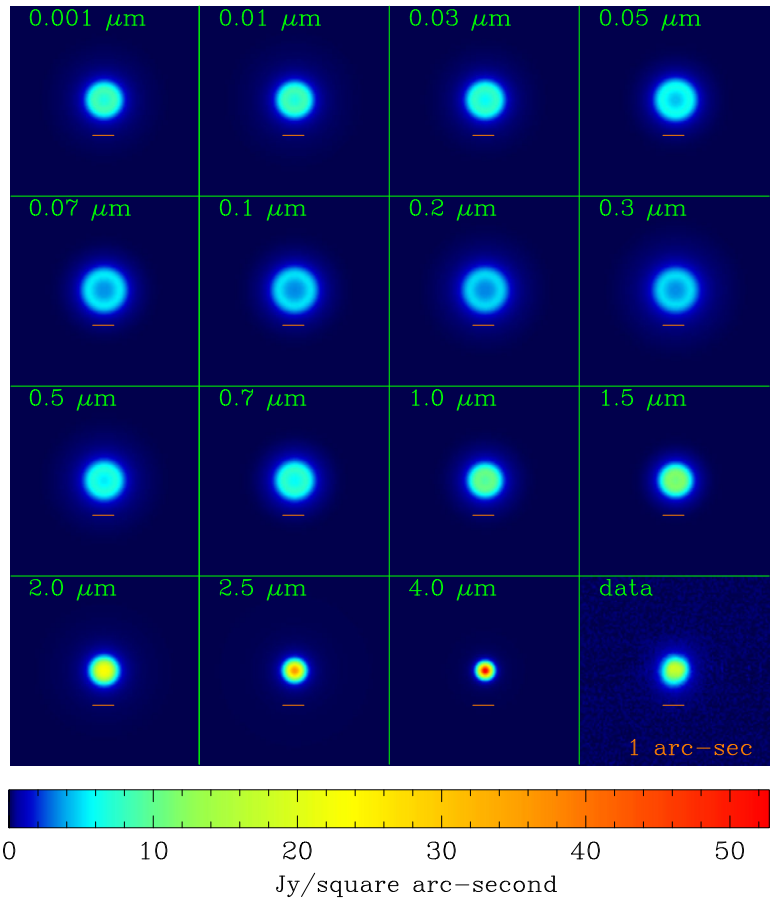

Fig. 4 Predicted surface brightness images at 22.1 μm, corresponding to the central wavelength of the T-ReCS Q filter, for IRAS 14325−6428, where for each grain size the model is fit the observed *Spitzer* spectrum. Small grain radii were found to require relatively large inner dust shell radii to avoid the dust getting too hot to match the observations. Also shown at lower right is the observed T-ReCS image after de-convolution with the PSF for the filter at the time of observation. The best match to the observed image is obtained at a dust radius of about 2 μm

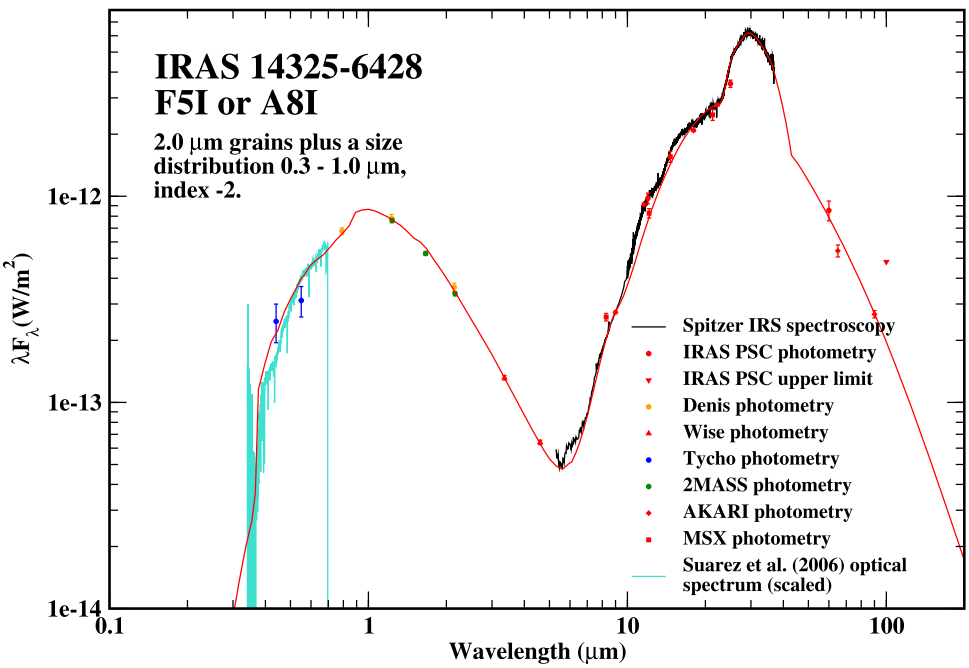

Fig. 5 This plot shows a dust radiative transfer model fit to the SED of IRAS 14325−6428 (the red curve), along with the available photometric and spectroscopic data used in the fitting. The fit to the SED also produces the correct image size and surface brightness at 22.1 μm as seen in Fig. 4. In this case, although the main dust population has radius 2.0 μm, a component of smaller dust sizes is present that produces emission at the shorter wavelengths, below 10 μm, to match the Spitzer data. The 30 μm feature is modelled in the same way as by Volk et al. (2011)

Table 1 Estimated dust radii for 30 μm sources where combined fitting of the SED and the thermal dust emission has been carried out. In all cases the dust modelling uses the BE amorphous carbon base cross-sections from Rouleau and Martin (1991) as the base dust opacity

Object name	Best fit dust radius (μm)	A_V (magnitudes)	τ_V	$\tau_{11.22\ \mu m}$
IRAS 07134+1005	0.3	1.15	0.66	0.00925
IRAS 14325−6428	2.0	2.7	0.56	0.345
IRAS 19500−1709	1.25	1.3	1.14	0.37
IRAS 22272+5435	0.005	2.2	0.86	0.017
IRAS 23304+6147	0.25	3.45	1.8	0.021

30 μm feature to be single-peaked as observed, based on models with a grain radius of 0.1 μm. Assuming that this thickness also applies to larger grains, one requires less MgS relative to the base grain material to provide a 0.1 μm coating for the large grain sizes determined for most of these objects. Such large sizes also are predicted to allow much more efficient MgS condensation onto the grains. On the other hand, for IRAS 22272+5435 the small derived grain size presents a problem for the coated grain model, given that this object has a strong 30 μm feature that carries about 30% of the infrared emission (Volk et al. 2002). The small grain size derived for IRAS 22272+5435 likely indicates that the base dust grains in this object are different from the BE type amorphous carbon grains assumed. At this small grain size, the model may be inaccurate due to quantum heating effects.

In the more general sense, the determinations of the grain sizes in these objects, as well as for NGC 7027 (Lau et al. 2016) and other similar PNe, generally lead to much larger grains than are derived for interstellar dust. While any of these determinations may be subject to systematic errors, it seems unlikely that all these objects have the small grains normally assumed for the ISM population. Hence, one should not simply assume the ISM size distribution in AGB or post-AGB objects without considering that the grains may be larger.

1.4 Other proposed carriers

While most of the discussion of the carrier of the 30 μm feature has concentrated on MgS and related compounds, a few alternatives have also been proposed. Papoular (2000, 2011) has suggested that molecules similar to the polycyclic aromatic hydrocarbons, but with various oxygen-bearing subchains, may produce the feature. The *Herschel* observations have clearly demonstrated that oxygen chemistry occurs even in carbon stars with a high C/O ratio. It is difficult to assess whether enough of these compounds can be produced to make the 30 μm feature with this proposed carrier, and in general this seems unlikely given that the feature is not often seen in S-type stars where both oxygen and carbon chemistry are likely to occur. Grishko et al. (2001) suggested that hydrogenated amorphous carbon produces the feature. These proposals have not received much attention in the literature. In the absence of detailed predictions for the feature shape and strength in these carriers, it is impossible to determine whether these are viable candidates. Nor do we know whether these carriers produce any other infrared features. Hence these alternatives proposed are not currently strong candidates.

One aspect of postulating a carbon-based carrier for the 30 μm feature is that its abundance would not depend as strongly on metallicity as MgS, because metal-poor carbon stars still produce carbon by the triple-alpha process. It is not clear whether the decline in the strength of the feature at low metallicities would be expected for these carriers.

1.5 Unresolved issues and future work

While the MgS hypothesis does appear to be able to explain the 30 μm feature, there remain issues in making definitive models on this basis. Simplified dust models using MgS have been successful in matching observed spectra, yet in many cases fine-tuning of the parameters is needed to provide enough MgS for the model given an assumed input sulfur abundance (e.g., Szczerba et al. 1999). The lack of proper optical constants for MgS grains is a fundamental limitation on any such modeling. Measurements of the optical constants of MgS in the optical and ultraviolet wavelength range are urgently needed so that self-consistent dust shell models can be produced using MgS grains.

Dust shell models by Volk et al. (2011) and those described in Sect. 1.3 assume that the carrier of the 30 μm feature is in thermal contact with the amorphous carbon grains, so that carrier, be it MgS or something else, is always physically associated with the dominant carbon grain throughout the dust shell as indicated by the available imaging. If MgS is always a thin coating on large amorphous carbon grains this assumption would automatically be satisfied. This empirical approach allows dust shells to be modeled, but it does not address the issue of sulfur abundance or give insight about grain coating. On the other hand, the simple models of a spherical (or ellipsoidal) grain of uniform composition, possibly with a uniform coating of another composition, is clearly an unrealistic idealization of what must be happening in the circumstellar shells of carbon stars. Allowing for the many extra degrees of freedom that come with abandoning the assumption of simple spherical grains in modeling is difficult because we do not have enough detailed information

to constrain the additional parameters that are introduced. The same is true in going from one-dimensional models for the dust shell to three-dimensional geometries. All of these factors should be used in the dust-shell models, but we do not generally have observations to allow us to determine, or even loosely constrain, all the extra parameters.

Two observational avenues are available that would provide new information about the carrier of the 30 μm feature. One is using resolved imaging to get learn more about the grain distribution. The second is using polarimetry to gain information about the grain shapes and resonances. Polarization observations should be able to immediately confirm or rule out the carrier being a dust grain, because molecules would not produce any polarization. To the authors' knowledge, polarization measurements of the 30 μm feature have not been published. While the desired observations are straightforward to describe, the small number of mid-infrared instruments currently on ground-based or airborne telescopes means that no such polarimetric instrument at 30 μm is available. The HAWC+ instrument on SOFIA only allows polarimetry at wavelengths longer than 50 μm. Polarimetry would reveal if two or more dust grain resonances form the observed 30 μm feature. That could address the possibility that multiple carriers, such as MgS, CaS, and FeS, are contributing to the feature.

For direct imaging, if we could obtain spectroscopy of nearby objects with high angular resolution or narrow-band imaging on and off the 30 μm feature, we could in principle determine whether the carrier of the feature and the carrier of the continuum (probably amorphous carbon) are well mixed in the dust shell. We could also determine if MgS condenses further out in the envelope than the amorphous carbon or SiC. The wavelength coverage of the Mid-Infrared Instrument (MIRI) on the James Webb Space Telescope (JWST) only extends to ∼28 μm, and observations from the ground will continue to be impractical, so we must await the next generation of infrared space telescopes.

1.6 Conclusions

The 30 μm feature is generally assumed to be due to MgS grains, and while there are still difficulties with this idea, it remains the best candidate that we have. However, the fundamental questions about the required abundance of Mg and S needed to form either grains or coatings still requires more attention. The wide variation in conclusions, from those who maintain that there is plenty of MgS available to make the feature to those who maintain that there is far too little MgS, is rather dismaying. The lack of correlation between sulfur depletion and the presence of the feature in Magellanic PNe is also a weakness for MgS as the carrier. If MgS is eventually ruled out it would leave us with only a few very speculative ideas for the carrier that have not been examined sufficiently with laboratory spectroscopy.

In evaluating the MgS hypothesis, what is needed is a more systematic effort to apply any tests to a large number of objects rather than simply looking at one object for a particular study of abundances or grain formation, as has generally been the case in the past. Another way to look at this problem is that we lack fundamental information about the formation and evolution of dust grains in these circumstellar envelopes. These types of calculations need to be placed on a better physical basis to see if we really can understand the formation of MgS grains or coatings. We need improvements both in the treatment of the micro-processes at the level of grain formation and coating as well as at the hydrodynamical level in describing the environment under which the grains form. The interaction of the pulsation of the star with the stellar wind, neither of which are likely to be truly spherically symmetric, introduces significant complexity. Facilities such as ALMA may shed light on these details in nearby carbon stars. None of this sort of work can be made definitive as long as we lack basic information about the optical properties of MgS that we need for modelling.

Finally, we need more work on the abundances of gas-phase sulfur and other elements to determine explicitly whether the formation of the 30 μm carrier corresponds to a depletion of sulfur, as well as whether the intrinsic sulfur abundance allows production of MgS in sufficient quantity to produce the observed feature. Similar measurements of the Mg abundance in the gas phase would also be useful, although it is expected that the S abundance is the limiting factor for MgS formation. Without abundance measurements we cannot definitively state whether MgS formation is efficient enough. Again, we need these measurements in large samples to avoid generalizing from one or two objects. Measurements of other sulfur molecules such as SiS may also shed light on the possible gas phase abundance of MgS using chemical models. While such predictions are a bit speculative when we do not have a complete knowledge of the detailed physical conditions of the gas, they should provide further constraints on how much MgS would be available in the gas phase in the absence of grain formation.

2 The 21 μm emission feature

The 21 μm feature is another long-wavelength feature seen in the spectra of a small fraction of the post-AGB sources that show the 30 μm feature. It can be observed from the ground at a dry site, such as Mauna Kea, but the best spectra to study it come from space-based telescopes. Although the 21 μm feature overlaps with a few photometric bands such as the W4 filter on the *Wide-Field Infrared Survey Explorer* satellite (hereafter *WISE*, Wright et al. 2010) centered at 22 μm and the 24 μm band on *Spitzer*, these bands are wide enough and the feature weak enough that it does not

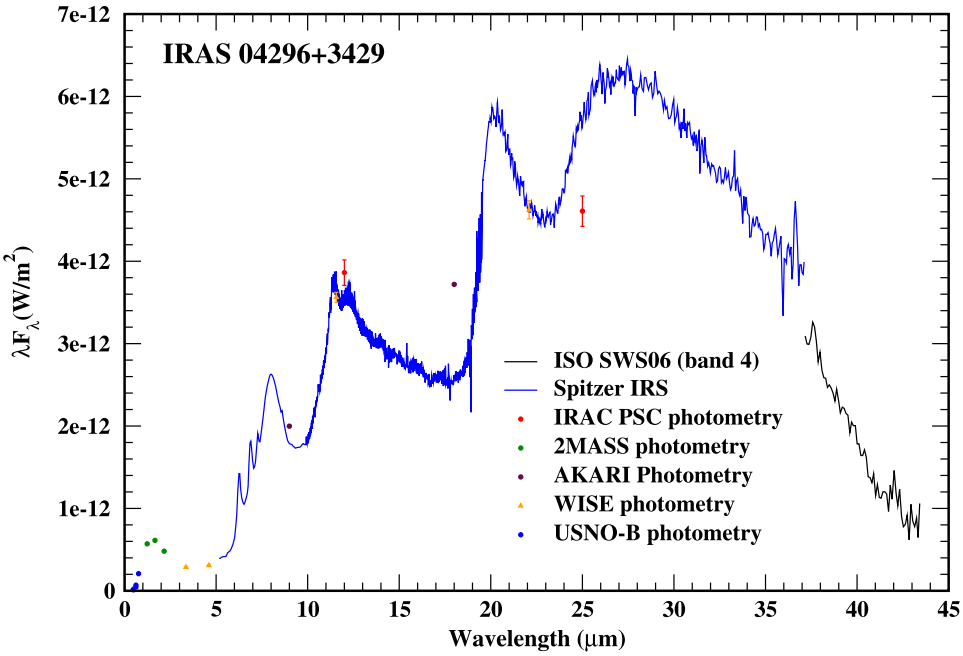

Fig. 6 An example of the 21 μm feature from *Spitzer*/IRS spectroscopy, along with photometric data. IRAS 04296+3429 was one of the original four *IRAS* objects in the discovery paper Kwok et al. (1989). One sees the complex hydrocarbon plateau and features between 5 and 15 μm, as well as the 30 μm feature. The 21 μm feature appears to start at ∼17.7 μm and extend to ∼23.4 μm

stand out in photometric surveys. As a result, we must rely on spectroscopy to detect it. As is the case for the 30 μm feature, this lack of spectral survey data makes the detection of the feature somewhat a matter of chance. Unlike the 30 μm feature, the 21 μm feature does not have a favoured candidate carrier.

The discussion will follow the same general outline as for the 30 μm discussion, first describing the feature and then discussing the possible carriers. The optical counterparts of the 21 μm sources are often bright, so we can also review their general stellar properties.

2.1 Observational properties

This feature was first detected by the Low Resolution Spectrometer (LRS) on *IRAS* (Olnon et al. 1986), but because the feature is rare and is situated just at the long-wavelength end of the LRS wavelength range, it was not initially recognized as a discrete feature in the LRS Atlas. The 21 μm feature was discovered only when the spectrum of IRAS 07134+1005 was extracted from the LRS database a few years later. Kwok et al. (1989) made that discovery and found three more objects with the same feature; all four were carbon-rich post-AGB objects.

Figure 6 shows an example of the feature using a spectrum from the IRS on *Spitzer* of IRAS 04296+3429. The feature actually peaks at 20.1 μm, but due to the low spectral resolution of the LRS and the relatively noisy spectra it was called the "21 μm feature". The shape of the feature is similar to that of the 10 μm silicate feature with a relatively steeper rise on the short wavelength side of the peak and a more gradual decline on the long wavelength side. The widths of the two features are similar as well. Because of the asymmetry of the 21 μm feature, its centroid (i.e. the wavelength with half the emission to either side) is at a longer wavelength than the peak, typically at ∼20.5 μm (Sloan et al. 2014).

Study of the feature shape is complicated by overlap with the short-wavelength wing of the 30 μm feature. On the short wavelength side of the 21 μm feature, another extended feature is often prominent and can affect the measured shape of the 21 μm feature. If one uses the inflection points to mark the short- and long-wavelength limits of the 21 μm feature, then it starts at 17.7 μm, peaks at 20.1 μm, and extends to 23.4 μm. Presumably the feature could be traced further in wavelength on both ends in a spectrum if additional features were not present. The nature of the features at shorter wavelengths will be discussed in the next section.

IRAS 07134+1005 (HD 56126) is the best-studied 21 μm source, and is generally taken to be typical of the group. The central star is bright and the circumstellar envelope is comparatively large on the sky as seen in mid-infrared images (e.g., Meixner et al. 1997). However, the central star may not be entirely typical compared to the other 21 μm sources, as discussed below. It is probably unwise to assume that results from HD 56126 automatically generalize to the other 21 μm sources.

Since the discovery paper, additional 21 μm sources have been identified in spectra from *IRAS*, *ISO*, and *Spitzer* (Garcia-Lario et al. 1999; Hrivnak et al. 2000, 2009; Cerrigone et al. 2011; Volk et al. 2011; Matsuura et al. 2014; Gladkowski et al. 2019). At present, the 21 μm feature has been firmly identified in 31 objects: 20 in the Galaxy, 9 in the LMC, and 2 in the SMC. Volk et al. (2011) identified six

Table 2 Cross-identification for IRAS 18370−0523

Survey	Catalogue	Position	Designation	Radius (″)
Gaia	DR2	18 39 43.675 −05 20 34.866	4256523529082834304	0.0
2MASS		18 39 43.69 −05 20 34.8	J18394368−0520348	0.2
MSX	6C	18 39 43.67 −05 20 34.8	G026.8436+00.1602	0.1
Spitzer	GLIMPSE I[a]	18 39 43.71 −05 20 34.5	SSTGLMA G026.8437+00.1600	0.6
AKARI	IRC V1	18 39 43.72 −05 20 33.5	J1839437−052033	1.5
WISE	AllWISE	18 39 43.69 −05 20 34.8	J183943.69−052034.8	0.2
Herschel	PACS 70 μm	18 39 43.56 −05 20 34.0	HPPSC070A J183943.5−05203	1.9
IRAS	PSC	18 39 43.27 −05 20 35.9	IRAS 18370−0523	6.1

[a]GLIMPSE: source is in GLIMPSE I Spring'07 Archive

21 μm sources in the LMC and one in the SMC using spectra from the IRS on *Spitzer*. Sloan et al. (2014) applied optimal extraction to produce spectra with better signal/noise ratios and were able to identify an additional three sources in the LMC and one in the SMC, plus three LMC targets with possible 21 μm features (see their Tables 1 and 16).

Claims of a weak 21 μm feature in three Galactic planetary nebulae (Hony et al. 2002; Pei and Volk 2003) and in three extreme carbon stars (Volk et al. 2000) are probably incorrect and due to artifacts in Bands 3D and 3E in spectra from the SWS on *ISO* (see the discussion of the *ISO* spectrum of IRAS 21318+5631 by Clément et al. 2005).

Finally, Chen and Shan (2012) identified IRAS 18370−0523 as a 21 μm source based on its LRS spectrum. The spectrum is fairly noisy, making this identification more tentative. Volk et al. (1991) judged that the object did not have a 21 μm feature when the spectrum was originally extracted from the LRS database. No specific follow-up observations have been published, but it does appear in multiple infrared surveys as listed in Table 2. The table includes a *Gaia* DR2 source close to the 2MASS position.[2] This source needs follow-up observations to verify the feature.

Additional identifications of 21 μm sources prior to the launch of *ISO* have not held up. Cox (1990) suggested that the LRS spectra of some compact HII regions showed a 21 μm feature, but the spectral structure they saw turned out to be an artifact caused by edge effects in the LRS spectra for extended objects. Later spectra from *ISO* and *Spitzer* revealed no evidence for 21 μm features in these sources. All other known sources of the 21 μm feature are carbon-rich, so its presence in oxygen-rich HII regions would have been quite the surprise. Buss et al. (1993) and Omont et al. (1995) reported a weak 21 μm feature in the Egg Nebula (AFGL 2688). Given its carbon-rich and post-AGB nature, the presence of the 21 μm feature seemed more reasonable, but the spectrum from the SWS on *ISO* does not show any features near 20 μm.

All of the 21 μm sources also show the 30 μm feature, and that feature is generally strong in the Galactic objects. IRAS 07134+1005 is an exception, with a weak enough 30 μm feature to lead some to question its presence (Raman et al. 2017), while others model its dust shell with the feature present (Volk et al. 2002). Objects in the Magellanic Clouds show a range of strengths of the 30 μm feature, but it is present in the spectra of all 21 μm sources. On average the 30 μm feature is weaker in Magellanic objects than in Galactic objects. The lone known SMC object with a clear 21 μm feature has only a weak 30 μm feature similar to that of IRAS 07134+1005 (Volk et al. 2011).

The shape of the 21 μm feature does not vary substantially from one object to the next, although small variations in the peak wavelength are seen (Volk et al. 1999). Volk et al. (2011) were able to fit all of the Magellanic objects from set template shapes for both the 21 μm and 30 μm features. The shape of the feature in the spectrum of the recently discovered source IRAS 18533+0523 may vary from other objects, as Fig. 7 shows. Detailed modelling is needed to assess this possibility.

Rho et al. (2008) found an emission feature at 21 μm in the Cas A supernova remnant (SNR), but the feature in this object is clearly distinct from the 21 μm feature seen in carbon-rich post-AGB objects. Rho et al. (2018) found a similar feature in another SNR, G54.1+0.3, which they describe as the "21 μm silicate dust feature". They can fit it and other features in the spectra with SiO_2 grains. This oxygen-rich feature peaks at 21.0 μm, compared to 20.1 μm for the carbon-rich feature. It is rather unfortunate that both features have the same name. Renaming the carbon-rich feature "the 20 μm feature" would help to avoid any confusion, but that would be a challenge 30 years after the initial discovery paper.

2.2 Other features in the infrared spectra

Most of the 21 μm sources show a number of other strong emission features in their spectra, in addition to the 30 μm

[2]The table excludes a Pan-STARRS detection very close to the *Gaia* DR2 position (objID 101582799320378824), but with photometry an order of magnitude brighter than expected from the *Gaia* and 2MASS photometry. The Pan-STARRS quality flag (qualityFlagvalue 104) suggests possible issues with the photometry.

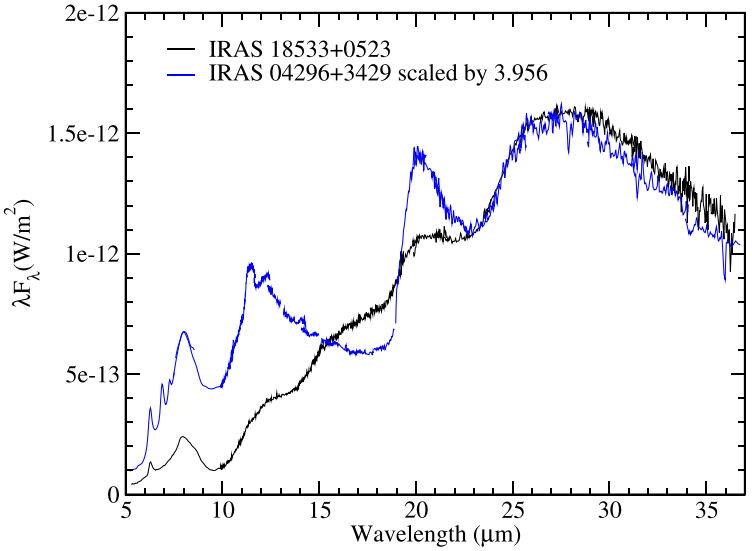

Fig. 7 The *Spitzer* IRS spectra of IRAS 18533+0523 compared to that of IRAS 04296+3429, with the latter spectrum scaled down (by a factor of 3.956) to match the continuum level of the former at the long-wavelength edge of the 21 μm feature. The shape of the 21 μm feature in IRAS 18533+0523 differs slightly from the usual profile, with the peak offset to a wavelength of about 20.2 μm and a possible small change in the slope of the rise at about 19.2 μm. The latter difference occurs near the boundary between two spectral segments in the high-resolution mode and should be considered with caution

feature. These additional features are common enough that Kraemer et al. (2002), when classifying spectra from the SWS on *ISO*, used the family of associated features discussed in this section as much as the 21 μm feature itself to identify the 21 μm sources. Out of the over 1,000 spectra obtained by the SWS on *ISO* in full-scan mode, they identified seven 21 μm sources firmly, with two more which they marked as uncertain, due to poor-quality data. It is likely that the two uncertain identifications, for CD−49°11554 (PN G341.4−09.0) and RAFGL 5385 (IRAS 17441−2411) are probably misclassified due to artifacts and discontinuities in their spectra.

2.2.1 Emission features from complex hydrocarbons

The 21 μm sources usually show the "unidentified infrared" (UIR) emission features commonly attributed to small grains composed of complex hydrocarbons. Gillett et al. (1973) first discovered these features in the spectra of carbon-rich PNe. They appear most commonly, as a group, at 3.3, 6.2, 7.6–7.9, 8.6, 11.3, and 12.7 μm (with additional features at longer wavelengths) and arise from a class of solid-state material commonly attributed to polycyclic aromatic hydrocarbons (PAHs; e.g. Leger and Puget 1984; Allamandolla et al. 1985, 1989; Tielens 2008). In the PAH model, the UIR features arise from particles which can be described as either very large molecules or very small grains. They are composed of planar molecules of ∼100 carbon atoms arranged in multiple interconnected hexagonal rings, each made of six carbon atoms, with hydrogen atoms bonded to the carbon at the edges. The C–C and C–H vibrational and bending modes in the infrared are excited in PAHs when they absorb UV or optical photons, and they can explain all of the observed UIR features from 3 to 13 μm.

Peeters et al. (2002) devised a classification system for sources with UIR features in their spectra from the SWS on *ISO*. The vast majority fall into Class A or B, with a small shift seen in the 6.2 μm feature to longer wavelengths from A to B. In Class A spectra, the 7.65 μm component dominates the 7.6–7.9 μm region, while in class B, the 7.85 μm component dominates. The general trend is for Class A spectra to arise from star-forming regions, and Class B spectra to appear in post-main-sequence objects like PNe. Numerous exceptions to this rule can be found, however.

A number of other hydrocarbon-rich carriers have been proposed for the UIR features, including hydrogenated amorphous carbon (HAC; see Jones et al. 1990, and references therein) and coal (Papoular et al. 1989). Kwok and Zhang (2013) provide a concise review of the proposed alternatives to PAHs, and argue that "mixed aromatic/aliphatic organic nanoparticles" (MAONs) is a better description of the carrier of the UIR features. Observational and laboratory evidence supports the idea that PAHs are often mixed with aliphatic hydrocarbons. Peeters et al. (2002) classified two spectra in their sample as Class C because of their differences with the rest of the sample. Both had shifted features, with the 6.2 μm feature appearing at 6.3 μm and the 7.6–7.9 μm complex shifted to ∼8.2 μm. Both were also carbon-rich post-AGB objects, including the Cygnus Egg (AFGL 2688). Sloan et al. (2007) examined several more Class C sources discovered with the IRS on *Spitzer* and found that all were associated with much cooler radiation fields than Class A or B sources. They hypothesized that a greater fraction of aliphatic hydrocarbons could explain the Class C emission. Pino et al. (2008) confirmed that hypothesis by showing that an increasing aliphatic/aromatic ratio in laboratory samples resulted in greater shifts of the emission features to longer wavelengths. Because the carrier of the UIR features contains a mixture of PAHs and aliphatic

hydrocarbons, we will describe it for the remainder of this paper as "complex hydrocarbons".

Spectra with the 21 μm feature often show emission features attributed to aliphatic hydrocarbons, but these features often also appear in the spectra from other carbon-rich post-AGB objects. Geballe and van der Veen (1990) and Geballe et al. (1992) found unusual emission at 3.3–3.4 μm, with an unusually strong 3.4 μm feature compared to the usually dominant 3.29 μm feature in three 21 μm sources, and moderately strong 3.4 μm emission in the Cygnus Egg, which is not a 21 μm source. The 3.29 μm feature arises from a C–H stretching mode in aromatic hydrocarbons, while the 3.4 μm feature arises from a similar C–H mode in aliphatic hydrocarbons (see Goto et al. 2003, for a good review of these assignments). Additional emission features from aliphatic hydrocarbons also appear at 6.85 and 7.25 μm, but as shown by Sloan et al. (2014) for Magellanic sources, while one or both of the features usually appear in the spectra of 21 μm sources, they are not always present, and they can often be seen in other carbon-rich post-AGB spectra as well.

Matsuura et al. (2014), in their study of carbon-rich post-AGB objects in the LMC, found several sources with emission features from complex hydrocarbons that required a new classification. They identified the Class D hydrocarbon spectrum based primarily on an unusual profile of the features at 7–9 μm. In most emission spectra from complex hydrocarbons, the emission components from C–C modes at ∼8 μm and the C–H in-plane bending mode at 8.6 μm are separated, so that the emission profile dips between them, but in Class D spectra, an additional component of unknown origin completely fills in this wavelength region.

Sloan et al. (2014) recognized that the Class D spectra were associated with two distinct feature profiles at 11–13 μm. This region includes multiple features from the C–H out-of-plane bending modes. Normally the solo mode at 11.3 μm dominates, with a weak duo mode at 12.0 μm and a moderately strong trio mode at 12.7 μm. In the Class D1 spectra, this region takes on a triangular profile, with the apparent strength of the 12.0 and 12.7 μm components reversed. The Class D2 spectra are similar, but the 12.0 and 12.7 μm components have been replaced with longer wavelength components at ∼12.4 and ∼13.2 μm.

Of the 11 Magellanic 21 μm sources examined by Sloan et al. (2014), six showed Class D2 hydrocarbon emission, three showed Class D1 emission, and two showed Class B hydrocarbons. Several carbon-rich post-AGB objects with no 21 μm feature also showed Class D1 spectra, but all of the D2 spectra were limited to just the 21 μm sources. These observations illustrate an important and somewhat frustrating characteristic of carbon-rich post-AGB spectra. While trends are readily apparent when looking at which features tend to appear alongside other features, no rule is without its exceptions. That lack of consistency makes it a challenge to quantify the apparent correlations we see among individual features in the spectra. The Galactic 21 μm objects have not yet been examined for the class D sub-types.

Additional emission features at 15.8 and 17.1 μm often appear in the spectra of 21 μm sources. Sloan et al. (2014) showed that the 15.8 μm feature can be produced by propyne, which is a short aliphatic hydrocarbon change which ends with a triple bond (C≡CH). Similar longer chains terminating with the same triple-bonded group produce a similar feature. Aliphatic hydrocarbons with triple bonds in their interior can produce the 17.1 μm feature. Thus both features may arise from aliphatic hydrocarbons.

2.2.2 The hydrocarbon plateaus

The discovery paper of the 21 μm feature (Kwok et al. 1989) noted that the LRS spectra of all four 21 μm sources show a relatively flat feature (in λF_λ units) from roughly 11 to 17 μm, which was assumed to be a broad emission feature of unknown origins.

The wider wavelength coverage of the SWS on *ISO* and spectra from *Spitzer* revealed that a number of broad emission features usually accompanied the 21 μm feature, leading to what Kraemer et al. (2002) described as a "step-like appearance" to the spectrum (when plotted in F_ν units). This character is particularly noticeable in the spectrum of IRAS 04296+3429 in Fig. 7. Both spectra in the Figure show multiple broad features, along with narrower hydrocarbon emission features at shorter wavelengths, including aromatics (at 6.3 μm) and aliphatics (6.85 μm), but they also differ in many ways.

While IRAS 04296+3429 shows a broad Class D-like feature at 10–17 μm, IRAS 18533+0523 shows two plateau-like feature at 10–14 and 14–18 μm. Many of the Galactic 21 μm sources show similar broad plateau-like features in place of the usual narrow emission features from complex hydrocarbons in the 10–14 μm region (e.g., Kwok et al. 2001). Some Galactic sources show just the plateaus (e.g. IRAS 07134+1004 and IRAS 22272+5435). Magellanic 21 μm sources usually show even stronger plateau-like features, but they are always accompanied by the narrower emission features, usually Class D, both at ∼8 μm and in the 11–14 μm region (Volk et al. 2011; Matsuura et al. 2014; Sloan et al. 2014).

Allamandolla et al. (1989) noted that the narrow emission features from complex hydrocarbons were often accompanied by broad emission plateaus, which they attributed to PAH clusters and larger particles more closely related to grains of amorphous carbon. Amorphous carbon dominates the dust emission in carbon stars on the AGB (e.g., Martin and Rogers 1987; Groenewegen et al. 2007), but it produces no identifiable spectral features, not even the broad plateaus seen in 21 μm sources (e.g., Rouleau and Martin

1991; Zubko et al. 1996). Thus the plateaus appear to arise from a grain intermediate between the amorphous carbon seen on the AGB and the aromatic hydrocarbon emission features seen in carbon-rich PNe. The 21 μm sources are intermediate between these two evolutionary stages, and their dust reflects that. If the complex aromatic hydrocarbons responsible for the family of narrow infrared emission features are produced by the breakdown of larger amorphous carbon grains, then the plateau-dominated spectra may be revealing a stage when that processing has not yet been completed.

Most of the Galactic 21 μm objects show only very weak individual hydrocarbon features. Instead, the board plateau features from 7 to 20 μm dominate (Hrivnak et al. 2000). In the Magellanic Cloud 21 μm sources, discrete features such as at 11.3 μm are stronger compared to the underlying plateaus. This difference in the spectra must reflect either some difference in the carriers of the features or differences in how they are radiationally excited. One possibility is that the ultra-violet radiation field is stronger in the Magellanic Clouds, due to the lower metallicity of the stars themselves, or from the interstellar radiation field (e.g. Paradis et al. 2009), or both.

The component analysis of the spectra of many of the 21 μm sources by Mishra et al. (2015), where a large set of Drude profiles are used to model the features, found no correlations between the various hydrocarbon emission features, the 21 μm feature, or the 30 μm feature. However, they fitted the 30 μm feature with up to three separate components, and as discussed previously, the *Spitzer* observations of the 30 μm feature show no instances with multiple peaks in this feature. The general association of the 21 μm feature with all of these molecular features has led to speculation that the 21 μm feature carrier is a molecule related to complex hydrocarbons, although it has not been found to correlate closely with any individual emission feature.

2.2.3 Absorption from molecular hydrocarbons

A subset of the 21 μm objects show a weak absorption band at 13.7 μm, which arises from the Q branch of the ν_4 band from gaseous acetylene (C_2H_2). IRAS 06530−0213 is an example. This band is commonly seen in the spectra of carbon stars, so it is not surprising that a remnant of it would appear in the 21 μm source spectra. High-resolution spectroscopy of a few of these objects in several individual C_2H_2 lines made with TEXES at Gemini North (Volk, unpublished) show strong P-Cygni line profiles. Figure 8 shows part of the TEXES spectra for two of the objects with the detected C_2H_2 lines marked. The radial velocities of the sources are +33 km/s for IRAS 06530−0213 and −67 km/s for IRAS 22574+6609 so one easily sees the relative line shifts at this resolution.

For IRAS 22574+6609 the spectrum clearly shows two isotopic lines of the molecule with substitutions of ^{13}C, as well as the normal form with ^{12}C, at a line strength ratio of ∼5 between the regular C_2H_2 line at 13.038 μm and the isotopic line at 13.070 μm . In the case of IRAS 06530−0213, the spectrum shows a tentative detection of the isotopic line at 13.074 μm with a line-strength ratio of ∼100 to the normal line. Although satisfactory molecular excitation models could not be made to match the observed spectra, to first approximation the $^{13}C/^{12}C$ abundance ratio is the same as the isotopic-to-normal line strength ratio. The indication is that IRAS 22574+6609 has a high $^{13}C/^{12}C$ ratio while this ratio is much smaller in IRAS 06530−0213. Another object observed, IRAS 05341+0852, showed a number of the C_2H_2 lines but not the isotopic lines, so presumably the $^{13}C/^{12}C$ ratio is also small in this object.

A high abundance fraction of ^{13}C is normal for the J-type carbon stars (see Abia and Isern 2000). A lower abundance fraction of order 0.01 is normal for the Class N carbon stars. The J-type carbon stars show significant enhancements in s-process elements, similar to what the 21 μm sources have, so one would expect the 21 μm sources to have a high relative $^{13}C/^{12}C$ ratio. This appears to be the case for IRAS 22574+6609 but not for the other two objects.

2.3 Stellar properties

2.3.1 Spectral types

Many of the 21 μm objects are associated with bright optical counterparts for which information about the central star is readily obtained. A number of papers have examined the spectroscopy of these stars starting with early work by Hrivnak (1995) as well as more recent surveys (e.g., Suárez et al. 2006; Sánchez Contreras et al. 2008). The central stars show the spectral signatures of low surface gravity with spectral types ranging from G9 I to B7 I. Most of the objects have spectral classes of F or G.

Two objects have been classified as cool supergiants in the past, IRAS 07430+1115 and IRAS 22272+5435 (e.g., Suárez et al. 2006; McCuskey 1955, respectively). However, those classifications were based on lower resolution spectra in which the C_2 absorption bands were not easily recognizable. Higher resolution data show the C_2 bands and suggest much hotter spectral types of G or F, more in family with the other 21 μm sources (e.g., Hrivnak and Kwok 1999; Hrivnak 1995).

Those stars studied with high-resolution spectroscopy show strong enhancements in s-process elements (e.g., Zacs et al. 1995; Decin et al. 1998; Reddy et al. 1999, 2002; Klochkova et al. 1999; Van Winckel and Reyniers 2000; De Smedt et al. 2012; van Aarle et al. 2013; De Smedt et al. 2016). The metallicity of the stars is typically sub-solar, [Fe/H] ∼ − 0.5 to −1.0. In most cases the stars also clearly have C/O ratios significantly larger than 1. A minority of

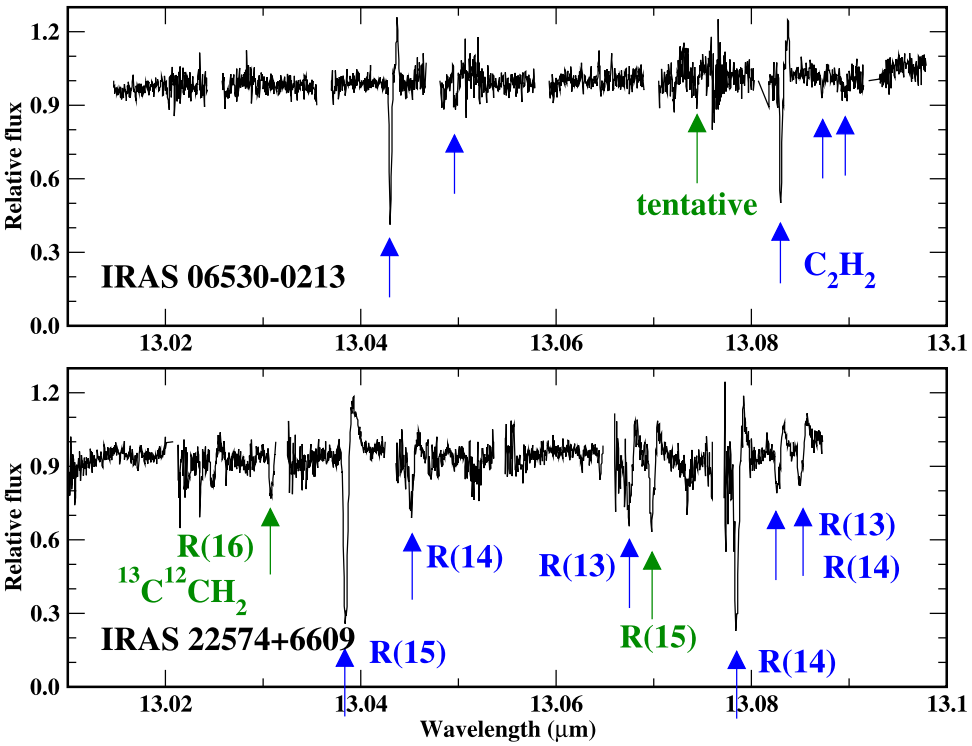

Fig. 8 High resolution mid-infrared spectra for two of the 21 μm objects taken with TEXES at Gemini North. The various C_2H_2 lines are marked with the arrows. The upper panel shows the spectrum for IRAS 06530−0213 and the lower panel shows the spectrum for IRAS 22574+6609. Lines marked by blue arrows are the regular C_2H_2 lines. The lines marked by dark green arrows are the ^{13}C isotopic lines. Two such lines are clearly detected for IRAS 22574+6609, although the emission component of the 13.0308 μm line is cut off by the edge of an echelle order. One possible very weak detection of an isotopic line may be present in the other spectrum

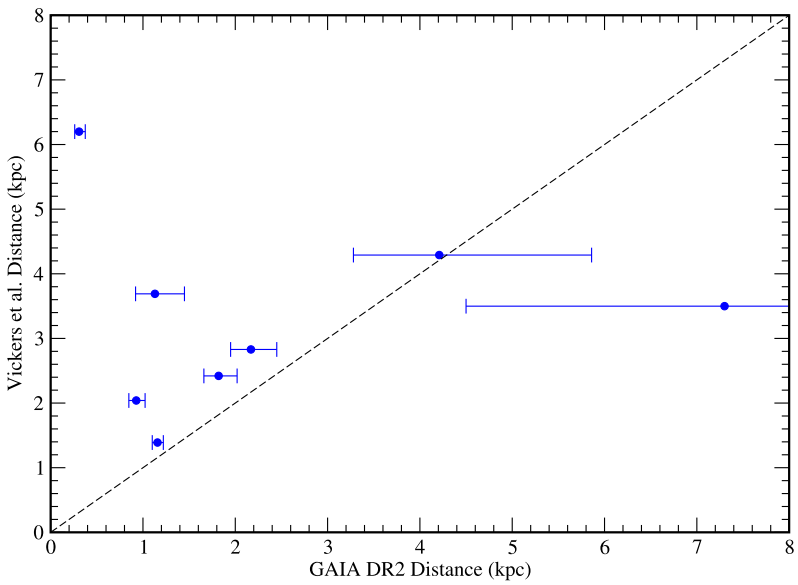

Fig. 9 A comparison of the *Gaia* DR2 estimated distances for eight 21 μm objects with relatively accurate parallaxes to the corresponding distance estimates from Vickers et al. (2015). The dashed line shows the 1:1 relation. Only one point of these eight is on the line within the Gaia DR2 1-σ uncertainties, and in that case the associated uncertainties are quite large. In general, it appears that Vickers et al. (2015) overestimate the object distances

21 μm sources in the Galaxy have derived C/O ratios ∼ 1 (within the uncertainties), which might suggest that the star had a spectral class of S or CS at the end of the AGB (e.g. HD 56126, Van Winckel and Reyniers 2000).

It is commonly assumed that the central stars have extended, low-mass atmospheres that result in the luminosity class I designation. Astroseismology could directly verify this assumption, but does not yet appear to have been done. Photometry of the stars shows low-amplitude variability due to multiple pulsation periods from ∼30 to ∼160 days (see Hrivnak et al. 2015 and references therein). Radial-velocity monitoring of a few of the objects reveals marginal evidence for a companion to IRAS 22272+5435, but not to three other 21 μm sources (Hrivnak et al. 2017).

None of the 21 μm objects have spectra types later than G9 (subject to the comment above about the two reports of M-type spectra). For post-AGB objects in general it has been difficult to find stars early in the evolution off the AGB. The lack of identified objects in this phase might be due to relatively rapid evolution while passing through the tempera-

tures associated with spectral class K, or it could be due to a selection effect against objects in this early stage. For the 21 μm sources, targets in this evolutionary stage would help address the question of whether the 21 μm feature is weak or not present at all when the star is cooler than G9.

On the other end of the temperature range, the 21 μm feature disappears sometime after the central object evolves to a spectral class of B and before it becomes a PNe. The central star in the young PN IRAS 21282+5050 is a carbon-rich object with spectral type [WC11] and hence is not that much hotter than IRAS 16594−4656 (class B7 I), but it lacks the 21 μm and 30 μm features. Another object that lacks the 21 μm feature but otherwise has a similar spectrum is IRAS 01005+7910, with a spectral class of B1.7 Ibeq (Klochkova et al. 2002). Such a star has an effective temperature of ∼21000 K, compared to an effective temperature of ∼12000 K for IRAS 16594−4656. One can postulate that the 21 μm feature disappears when the star is somewhere in this temperature range, although we cannot say for certain whether the spectra of IRAS 01005+7910 or IRAS 21282+5050 ever had the 21 μm feature.

2.3.2 Distances and luminosities

The second *Gaia* data release (Gaia DR2; Brown et al. 2018) provided parallax data for a number of the 21 μm sources, although high-quality parallaxes are only available for a few. Table 4 lists the available parallax values for the Galactic objects, estimated total fluxes calculated from the available photometry and infrared spectroscopy, extinction values for each object from Vickers et al. (2015), and the resulting estimated luminosities. The listed uncertainties in the distances and luminosities are calculated from the parallax uncertainties in *Gaia* DR2. Where the parallaxes are consistent with zero within the quoted uncertainty, the table gives only a lower limit to the stellar distance and hence the luminosity. Three objects have no *Gaia* DR2 parallax measurements, and for these objects only the corrected total fluxes are listed. The luminosities can be compared with the values for the Magellanic objects from Volk et al. (2011, their Table 8), which were calculated in a manner consistent with the values in Table 4. Estimating the interstellar extinction to these objects is generally difficult because they are all subject to a combination of interstellar and circumstellar reddening, and the latter is usually estimated to dominate.

The one clearly anomalous result is the distance of 308^{+67}_{-47} pc for IRAS 07430+1115. Given the corrected total flux observed from this object, the distance required to produce a luminosity of 4300 $L_\odot$, the average value of the other objects with luminosities that are not upper limits, would be 4.63 kpc. It is likely that the optical star is the counterpart to the infrared source, because it is only 0.6″ from the *WISE* position in a field of low stellar density and has rather unusual properties such as s-process element enhancement. The nominal luminosity of the source is only 19.1 $L_\odot$, far too low for the spectral type. The expected interstellar reddening at this position is only E(B−V) = 0.04 magnitudes,[3] and that is the value adopted for dereddening the photometry, so one cannot explain this large discrepancy in luminosity as due to interstellar extinction.

The other surprise is the small measured parallax for IRAS 23304+6147, which leads to a lower limit for the luminosity of 99000 $L_\odot$. That is much too bright for a post-AGB star under our current understanding of stellar structure and evolution. The lower limit for IRAS 20000+3239 is also somewhat higher than expected, although it is within the range observed in the Magellanic objects.

A few of the objects with reasonably accurate *Gaia* parallaxes still have low estimated luminosities under 2000 $L_\odot$, as for IRAS Z02229+6208 and IRAS 16594−4656. Two objects with relative parallax uncertainties under 15%, IRAS 07134+1005 and IRAS 22272+5435, have estimated luminosities near 4500 $L_\odot$ and so appear to have lower core masses than expected even for a post-AGB object in the thick disk population. In the latter two objects it is possible that the *Gaia* parallaxes will be revised down enough (by 3 or 4 times the current quoted uncertainty) that the estimated luminosities will fall in the range 6000–8300 $L_\odot$ normally assumed for these stars, but for the first two objects that is less likely given that the luminosity discrepancy is a factor of 3–4.

Reconciling the luminosities derived from the *Gaia* parallaxes and the observed fluxes for these objects with the predictions of stellar evolution models may be difficult. There are three possible ways to reconcile the observations with the predictions: the estimated distances may be too small, the interstellar extinction effects may be larger than has been assumed, or the estimated fluxes may be too small. Each of these possibilities has difficulties.

Roughly half the stars are bright enough to possibly have saturation issues in the *Gaia* photometry observations (G ∼ 12 or brighter, see Evans et al. 2018). The saturation might also affect the parallax values. Lindegren et al. (2018) discusses the *Gaia* DR2 parallax solution and notes that increased errors occur for G < 6, but no indication was given that this produces systematic errors in the parallaxes. The brightest of the 21 μm sources are two magnitudes fainter than G=6. Thus the *Gaia* parallaxes and their uncertainties should be reliable despite saturation effects on the photometry. We will need to wait and see whether future *Gaia* data releases produce significant changes in the measured parallaxes, but currently we have no indication that these measurements are systematically too high for the 21 μm sources.

[3] See https://irsa.ipac.caltech.edu/applications/DUST.

Table 3 Proposed Carriers of the 21 μm Feature

Proposed Species	References
FeO, Fe_2O_3, Fe_3O_4	Cox (1990), Posch et al. (2004)
$CO(NH_2)_2$ [Thiourea]	Sourisseau et al. (1992)
SiS_2	Goebel (1993)
fullerenes	Webster (1995)
nano-diamonds	Hill et al. (1998)
nano-TiC grains	von Helden et al. (2000)
coal + O side-groups	Papoular (2000)
hydrogenated amorphous carbon (HAC)	Buss et al. (1990)
nano-SiC/doped SiC	Speck and Hofmeister (2004)
Ti + fullerenes or PAHs	Kimura et al. (2005)
PAH-like molecules	Papoular (2011)

Table 4 Distances and luminosities for the Galactic 21 μm Sources

Object	*Gaia* DR2 Parallax (0.001″)	*Gaia G* Magnitude	E(B−V)	Corrected Flux (W/m^2)	Distance (kpc)	Luminosity ($L_\odot$)
IRAS Z02229+6208	1.08±0.10	10.383±0.008	0.74	$8.14\ 10^{-11}$	$0.927^{+0.096}_{-0.080}$	2179^{+430}_{-390}
IRAS 04296+3429	−2.46±0.69	12.954±0.003	0.71	$8.94\ 10^{-12}$		
IRAS 05113+1347	0.11±0.21	11.478±0.008	0.38	$4.39\ 10^{-12}$	>3.2	>1400
IRAS 05341+0852	0.08±0.29	12.575±0.002	0.29	$2.44\ 10^{-12}$	>2.7	> 554
IRAS 06530−0213	−0.005±0.214	12.788±0.003	0.80	$5.15\ 10^{-12}$		
IRAS 07134+1005	0.46±0.05	8.055±0.002	0.07	$3.13\ 10^{-11}$	$2.17^{+0.28}_{-0.22}$	4600^{+1300}_{-900}
IRAS 07430+1115	3.24±0.58	11.595±0.003	0.04	$6.44\ 10^{-12}$	$0.3082^{+0.067}_{-0.047}$	$19.06^{+9.2}_{-5.3}$
IRAS 11339−6004	−1.08±1.58	19.383±0.013	0.35	$2.75\ 10^{-11}$		
IRAS 13245−5036	0.02±0.05	12.124±0.003	0.20	$1.01\ 10^{-12}$	>13.4	>5640
IRAS 14429−4539		13.241±0.005	0.15	$8.21\ 10^{-12}$		
IRAS 15482−5741	0.02±0.05	18.713±0.009	0.55	$1.69\ 10^{-12}$	>13.9	>10200
IRAS 16594−4656	0.88±0.20	14.892±0.006	0.51	$4.89\ 10^{-11}$	$1.13^{+0.32}_{-0.21}$	1940^{+1300}_{-650}
IRAS 18533+0523			1.00	$2.01\ 10^{-12}$		
IRAS 19477+2401	−2.46±0.87	18.445±0.008	0.80	$9.76\ 10^{-12}$		
IRAS 19500−1709	0.55±0.05	8.425±0.001	0.18	$5.40\ 10^{-11}$	$1.82^{+0.20}_{-0.16}$	5570^{+1300}_{-950}
IRAS 20000+3239	0.14±0.08	11.636±0.006	0.80	$1.71\ 10^{-11}$	$7.3^{+11.4}_{-2.8}$	>10700
IRAS 22223+4327	0.24±0.07	9.737±0.003	0.15	$1.27\ 10^{-11}$	$4.21^{+1.65}_{-0.93}$	7005^{+3600}_{-2700}
IRAS 22272+5435	0.86±0.05	8.084±0.008	0.65	$1.06\ 10^{-10}$	$1.158^{+0.063}_{-0.057}$	4440^{+480}_{-410}
IRAS 22574+6609			1.58	$6.26\ 10^{-12}$		
IRAS 23304+6147	0.004±0.059	11.781±0.001	0.80	$1.28\ 10^{-11}$	>15.7	>98500

Note. — The E(B − V) values are from Vickers et al. (2015). The total flux values are after correcting for the assumed extinction. The luminosity values have uncertainties from the distance estimate, but not from the flux calculation as the uncertainties in the total flux are difficult to determine. In general the photometric uncertainties are under 5% per point, hence assuming that the integrated flux has a similar uncertainty the distance uncertainties are the largest factor in the luminosity uncertainty.

The ISM extinction values from Vickers et al. (2015) are consistent with other estimates in the literature for these objects, hence there is no reason to think that these are systematically too low. For the objects at moderate Galactic latitude the extinction values are expected to be low and there is little prospect that the E(B−V) value is several times higher than what is assumed. Also, a number of the objects have estimated distances of order 1 kpc and fairly large assumed extinction values for such a distance (A_V values of 2.5 or more magnitudes). These are already higher than is normally assumed for most lines of sight for distances within 1 kpc of the Sun. Postulating even higher A_V values to provide an ex-

tra factor of 2 or more reduction in the stellar flux becomes difficult to justify.

Finally, we may be missing flux from the SED due to dust shell geometry effects. Some of the objects are clearly subject to such effects as can be deduced from the SED and the available optical and mid-infrared images. IRAS 16594−4656 is an example of this: the mid-infrared images show a narrow emission region plus bi-polar lobes, and the stellar part of the SED only carries about 1% of the total flux. In that case, the low derived luminosity is clearly at least partially due to geometrical effects hiding much of the stellar flux at our angle of view. The SED would presumably look quite different it viewed along the bi-polar lobes rather than along the waist of the dust shell. One would expect a much stronger stellar component to the SED and a larger observed flux for such an angle of view.

This does not appear to be the case for all the objects, as many show elliptical morphology in the infrared images and a prominent stellar peak in the SED. For these objects, SED modelling generally shows that the dust shells are optically thin in the mid-infrared, and in such cases one cannot hide much flux due to our angle of view to the star. Thus the hypothesis that we are systematically missing flux from the objects due to our angle of view appears to have problems.

Although some of the objects have low estimated fluxes due to asymmetric in the dust shells and our angle of view that hides the star, if we are viewing the systems at random angles then we should not see a systematically low set of flux estimates for all the objects. The mean estimated luminosity of the sources with reasonably accurate *Gaia* parallaxes is ∼4300 $L_{\odot}$, a factor of 1.5 to 2 below the range expected from theory. At present it is not clear how this discrepancy can be resolved. In the next few years the *Gaia* parallax measurements for most of these stars should improve to the point where we can rule out parallax errors as a significant source of uncertainty in the luminosity values, at which point this issue should be reconsidered.

Clearly many of the negative or noisy parallax measurements from *Gaia* DR2 need to be refined with additional *Gaia* observations, but the situation is much better than it was previously when no reliable distances were available. The *Gaia* parallax distances in general differ substantially from previously derived distance values. The estimates by Vickers et al. (2015) represent the best effort prior to *Gaia*, but as Fig. 9 shows, they differ significantly from the *Gaia* results. Their assumptions were reasonable, and their analysis was sound, but in general their distances appear to be too large.

2.4 Proposed carriers of the feature

Table 3 lists the many carriers proposed for the 21 μm feature. In the discovery paper, Kwok et al. (1989) did not propose any specific carrier, but they speculated that a type of carbonaceous grain might be responsible because the sources all seemed to be carbon-rich, as was soon verified by optical spectroscopy.

2.4.1 FeO dust

Cox (1990) proposed FeO as a candidate for the carrier because it has a resonance near 21 μm, and they thought at the time that the 21 μm feature could appear in the spectra from H II regions, which are oxygen-rich (see Sect. 2.1). We now know that the 21 μm feature only appears in carbon-rich objects, but FeO still appears among the list of candidate carriers. For example, Posch et al. (2004) suggested it as a possible carrier, while also noting the challenge of forming an oxide-based grain in a carbon-rich environment. Zhang et al. (2009) suggested that FeO was the best candidate for the carrier, but Mishra et al. (2016) no longer suggest any specific carrier for the 21 μm feature.

Observations from *Herschel* have revealed some oxygen-rich molecules even in environments with large C/O ratios (e.g., Decin et al. 2010). This is attributed to chemistry driven by the dissociation of CO molecules by the interstellar radiation field in the region close to the star, possibly within the dust formation radius. Observations of H_2O lines from a sample of eight carbon stars has shown that the abundance of H_2O is relatively small and varies significantly from one object to another (Neufeld et al. 2011). With such small amounts of H_2O present it is unclear that significant amounts of FeO can form. If FeO dust is somehow made in a carbon-rich envelope, it remains to be explained why the 21 μm feature does not appear in oxygen-rich environments, where FeO could form more readily.

FeO remains a good candidate for the 21 μm feature observed in supernova remnants (Rho et al. 2008, 2018). However, attributing that feature to FeO rules it out as the carrier of the 21 μm feature seen in carbon-rich environments because the two features are clearly distinct.

2.4.2 SiS_2

SiS_2 is another proposed carrier of the 21 μm feature (Goebel 1993). The simpler molecule SiS is observed in S stars on the AGB, both in absorption (Cami et al. 2009) and emission (Sloan et al. 2011), making SiS_2 at least plausible as a candidate. It does produce an emission feature near 20 μm, but it also has other strong features in the infrared that are not observed (Kraus et al. 1997). The emission feature from SiS_2 peaks at 22.5 μm, making its profile a poor match to the observed 21 μm feature. Many other candidates also fare poorly in fitting the 21 μm feature.

2.4.3 TiC

Von Helden et al. (2000) proposed very small TiC grains as the carrier of the 21 μm feature, and the shape and position

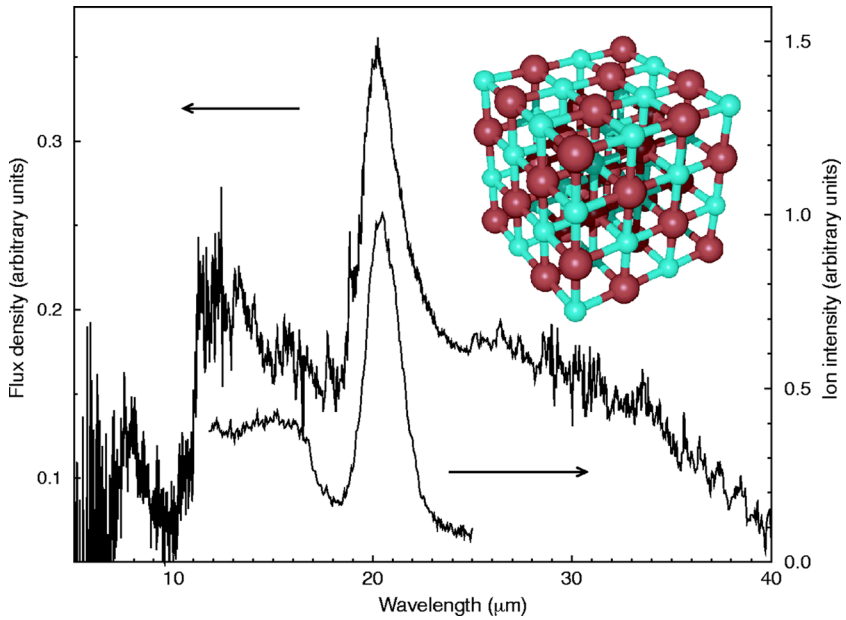

Fig. 10 Comparison of laboratory data from TiC nano-clusters and the 21 μm feature, reproduced from Fig. 1 of von Helden et al. (2000). The match of the laboratory feature shape to the observed feature is quite impressive

of the feature as measured in the laboratory fits the astronomical features very well. Figure 10 reproduces their Fig. 1 and compares the shape of the nano-TiC feature with the observed 21 μm feature. As the grains of TiC grow larger, the feature weakens and shifts to ∼19 μm (Speck and Hofmeister 2004). The detection of pre-solar TiC grains in meteorites (e.g., Bernatowicz et al. 2005) strengthens the case. The pre-solar TiC grains are generally small, but not as small as assumed by von Helden et al. (2000). They discuss the difficulties of forming TiC grains under the low-density conditions expected in circumstellar envelopes, and they suggest that the grains only form in a brief period of intense mass-loss right at the end of the AGB phase, so as to raise the density to the levels needed for the formation of TiC.

Li (2003) raised the concern that abundances may prevent the formation of enough TiC to explain the 21 μm feature. And formation issues remain formidable (Chigai et al. 2003; Meixner et al. 2004). In particular, the CO observations by Meixner et al. (2004) do not support the presence of the high-density environment needed to form the TiC grain. On the other hand, it is awkward to assert that TiC grains cannot form around carbon stars when we observe TiC in pre-solar grains which most likely were produced by carbon stars. If we simply assume that the existence of pre-solar grains of TiC demonstrates that small TiC grains can form with reasonable efficiency in (at least some) carbon stars, even if we do not understand the mechanism, then it remains possible that TiC produces the 21 μm feature. In their review of pre-solar grains, Alexander (2009) noted that the existence of large SiC and graphite pre-solar grains in meteorites is inconsistent with the normal view of dust formation in a steady outflow and instead requires a higher-density environment for formation. These conditions may also apply to forming TiC grains.

Questions remain about whether a sufficient number of small TiC grains can be formed and not subsequently be coated by SiC or graphite, which would quickly erase the emission feature. The grains could also be blown out by the stellar radiation pressure if they are not strongly coupled to the gas. Alternatively, very small TiC grains could be formed actively in the post-AGB phase by breaking down larger TiC grains in a shock. That might account for the transient nature of the 21 μm feature, as the TiC feature would be much weaker and at shorter wavelengths for larger TiC grains, or hidden by a coating, before the grains are broken into nanoparticles. However, this scenario is not consistent with the observation from the resolved images that the 21 μm carrier is well mixed with the bulk grains producing the continuum (see Sect. 1.3 above). In the end, despite the excellent match of laboratory samples the observed shape of the feature, the TiC hypothesis remains uncertain.

2.4.4 Nano-diamonds

Nano-diamonds are another pre-solar grain observed in meteorites that have been proposed as the carrier of the 21 μm feature (Hill et al. 1998). Meteoritic samples of nano-diamonds can produce an emission feature at ∼22 μm, but the feature does not arise from pure diamond crystals. Hill et al. (1998) hypothesize that lattice defects due to either the presence of nitrogen atoms or the removal of carbon atoms, perhaps from irradiation by neutrons, can produce the observed feature. Such grains produce features near 3.4–3.5 μm and have been proposed as a carrier of the extended red emission observed in many carbon-rich post-AGB objects and planetary nebulae (see the review by Chang 2016).

To date, no paper has published a laboratory spectrum showing the nano-diamond feature near 22 μm reported by Hill et al. (1998). Additionally, the features at 3.4–3.5 μm do not appear in the spectra of the 21 μm sources. Hence this identification remains tentative, at least until more supporting evidence becomes available.

2.4.5 Nano-SiC grains

Speck and Hofmeister (2004) proposed that very small SiC grains produce the 21 μm feature. Laboratory measurements of nano-SiC grains as well as thin films of the α and β lattice structures show a feature near 21 μm with a shape similar to the observed 21 μm feature, although in all cases, the peak wavelength is too long to match the observed feature. The emission from nano-SiC grains peaks at ∼21.2 μm, while the peak in the β-SiC sample is rather weak but much closer to the observed peak wavelength of the astronomical feature. They suggested that the cooling and processing of SiC grains in the post-AGB phase produces the 21 μm feature, which explains why the feature is not seen in carbon stars. Those stars are still on the AGB, and they typically show a strong emission feature from SiC dust at ∼11.5 μm.

The 11.5 μm SiC feature presents a challenge for the nano-SiC hypothesis. In the laboratory spectra that produce a feature near 21 μm, the 11.5 μm feature is much stronger, but in the astronomical objects, the 21 μm feature is either as strong as the 11.5 μm feature or much stronger. In some of the observed spectra, part of the emission in this region is due to the 11.3 μm feature and associated plateau from complex hydrocarbons. It is possible for the Class D profiles that SiC is contributing, as it does in young carbon-rich PNe (Bernard-Salas et al. 2009; Sloan et al. 2014).

The opacity of nano-SiC at 21 μm is also a problem. As Zhang et al. (2009) have argued, the nano-SiC hypothesis could require more Si than available to produce the observed strength of the 21 μm feature.

2.4.6 Fullerene and related material

The remaining proposed carriers are hydrocarbon molecules. The lack of resolved structure in the feature has generally been taken as evidence that it is due to a solid-state material. The highest-resolution spectra covering the 21 μm feature are from the SWS on *ISO*. The spectral resolution of the SWS at 21 μm is ∼1000 (it varied with wavelength, the observing mode, and how the data were reduced, leading to variation in the reported resolution in the literature), enough to marginally resolve the structure of the 8 μm SiO fundamental absorption band in cool giants (Sloan et al. 2015). PAHs can be described as a material at the boundary between large molecules and small grains, but that is primarily due to the physics of the fluorescence process where the absorption of a UV photon will temporarily heat the particle, which then cools through radiating at its infrared resonances (Sellgren 1984; Allamandolla et al. 1985). The particles must be small, but they are not so small that the emission feature at 3.3 μm can be resolved into molecular-band structure (Grasdalen and Joyce 1976; Tokunaga and Young 1980). The same would need to apply to the proposed hydrocarbon carriers of the 21 μm feature.

The Medium-Resolution Spectrometer (MRS) due for launch on JWST will obtain spectra with a spectral resolving power of ∼1500 at 15 μm, which will provide a better test (Wells et al. 2015). Spectra at much higher resolution are possible with instruments such as EXES on SOFIA (Richter et al. 2018). Such observation would definitely settle the question of a solid-state versus a molecular carrier.

One of the more interesting proposed carriers of the 21 μm feature at the boundary between molecules and grains is Ti bound to fullerenes (Kimura et al. 2005). The shape and central wavelength of the feature vary depending on how the sample is produced, and one variant produces a feature similar to the nano-TiC feature, making it a reasonable match to the observed feature. However, the same concerns about the Ti abundance raised for the TiC grain hypothesis also apply to this carrier (Zhang et al. 2009).

Prior to the proposal of Ti bonded to fullerene, Webster (1995) suggested that fullerene by itself could produce the 21 μm feature based upon theoretical band calculations. They found that in a variety of fullerenes the lowest-energy vibrational transition would be in the 19–23 μm wavelength range. That was well before the detection of fullerenes in *Spitzer* spectra (Cami et al. 2010). Although this possibility cannot yet be ruled out, the absence of emission features from fullerenes in the *Spitzer* spectra of 21 μm sources is a problem. In their study of carbon-rich objects evolving from the AGB to mature PNe, Sloan et al. (2014) found that the 21 μm sources and sources showing fullerenes in their spectra were mutually exclusive with the 21 μm feature appearing in objects with cooler central stars and the fullerenes appearing only in more evolved PNe with hotter central objects and clear forbidden lines in their spectra. Subsequently, Justtanont et al. (1996) suggested hydrogenated fullerenes as a possible carrier of the 21 μm feature, but at present, that hypothesis cannot be verified by the available observations.

2.4.7 The relation to complex hydrocarbons

As noted previously, finding a quantitative correlation between the 21 μm feature and individual spectral features from complex hydrocarbons, including the narrow features from aromatics and aliphatics and the broad plateaus, has proven challenging because every apparent relation comes with major exceptions. Cerrigone et al. (2011) propose a general correlation between the combined hydrocarbon feature emission from about 5 to 20 microns and the 21 μm

feature strength (their Fig. 8). However, they correlated raw flux values without correcting for distance. Making this correction removes the impact of nearby sources having apparently strong emission at both 21 μm and in the known hydrocarbons and more distant sources having weaker emission in both components. While the case for a strong quantitative correlation between the 21 μm feature and emission from aromatic and aliphatic hydrocarbons may be lacking, the qualitative relation between them is clear enough.

A few complex hydrocarbon carriers for the 21 μm feature have been proposed. Sourisseau et al. (1992) investigated a variety of coal-like substances and related smaller molecules and proposed thiourea, $CO(NH_2)_2$, as the carrier of the 21 μm feature. They presented a profile of the feature, extending from ∼16.5 to ∼25 μm and showing a peak at ∼20.5 μm. While this range is a bit larger than what is observed, a larger concern is that the molecule also produces a broader secondary peak at 22.5 μm which is not seen in spectra from *ISO* or *Spitzer*. This missing companion feature makes thiourea an unlikely candidate.

Coal-like particles with oxygen side-chains are another proposed carrier (Papoular 2000). A related idea involves large PAH-like molecules (Papoular 2011). These suggestions are based upon theoretical energy-level simulations, but no infrared spectroscopy has been published to verify these calculations.

All of these suggestions remain speculative and are neither supported nor ruled out by the available observations. The suggestions are interesting in that they are generally examining the regime between large molecules and small dust grains. If the carrier is carbon-based, as seems likely, then the richness of carbon chemistry means that the number of possibilities is quite large.

2.5 Why is the feature transient?

One of the most intriguing aspects of the 21 μm feature is how it is limited to such a narrow evolutionary range. It has not been convincingly detected in carbon stars on the AGB, nor has it been seen in PNe. It only appears in transition between these two stages. The suggestion by von Helden et al. (2000) that TiC only forms right at the end of evolution on the AGB might explain why the feature is not seen in carbon stars, but it does not explain why the feature disappears before the object evolves into a PN.

The differences in the spectra of 21 μm sources in the LMC and SMC compared to the Milky Way (see Sect. 2.2.1) point to differences in the evolution of the stars and their spectra in these galaxies. The lower metallicities in the LMC and SMC may be the root cause. The Magellanic spectra generally show weaker 21 μm features than in the Galaxy, which may indicate that metallicity directly affects the formation of the carrier. The smaller Magellanic samples leave us with no information about the behavior of the 21 μm feature at higher stellar temperatures. As for the relative numbers of 21 μm sources in the different systems, the many selection effects in both the Galactic and Magellanic samples make it difficult to draw conclusions.

As previously noted, where resolved imaging is available for these 21 μm sources objects it appears that the feature carrier is uniformly mixed through the circumstellar envelope. In such a case the carrier should still be present in the neutral shells of PNe, and one would expect to detect it. On the other hand, in young PNe like NGC 7027, hot dust grains dominate the emission at 20 μm, either from inside or at the edge of the ionized region. If the carrier of the 21 μm feature is destroyed when exposed to a shock or the UV radiation of the ionized region, then at best only a weak feature would appear from the much cooler dust in the neutral region. The possible detection of weak 21 μm features in three PNe is important in assessing this type of hypothesis. One sees changes in the 30 μm feature in the spectra from post-AGB objects and PNe, so perhaps both types of grains are being processed and the 21 μm carrier is affected more strongly and thus becomes too weak to readily observe.

Another possibility is that the carrier of the 21 μm feature is a material that is first produced or excited when the star evolves to a spectral type of roughly G, the most likely reason being that at least a small amount of UV radiation is needed to produce the carrier or excite the feature. Nonetheless, it remains very puzzling that the feature disappears rapidly when the central star evolves to a spectral class of B. If the carrier were a very small particle or a large molecule, it might become reactive when excited and thus be removed from the envelope. Or it might simply be destroyed radiatively. If the carrier were an aliphatic hydrocarbon, one would expect it could disappear due to photo-processing, because aliphatics are not observed in carbon-rich PNe. When making the case for SiC grains as the carrier of the 21 μm feature, Speck and Hofmeister (2004) suggested that processing of the grains would be expected and would explain the transient nature of the feature.

One way to test this type of idea would be to use integral field spectroscopy over the feature in a few of the 21 μm objects and a few young PNe to search for small-scale variations of the carrier of the 21 μm feature from the dust grains that produce the continuum, or to detect a weak 21 μm feature at a position within a young PN. Observing any separation of the 21 μm feature carrier from the continuum dust carrier has not proven possible from ground-based observations with of order 0.4″ angular resolution, but it might become possible using MIRI on JWST with its higher spectral and spatial resolution.

One other way to probe the 21 μm feature is to look in detail at a few of the objects that closely resemble the 21 μm sources but which lack the feature. This approach

could potentially identify basic differences between objects with and without the feature. The Galactic objects IRAS 01005+7910 and IRAS 17441−2411 are prime candidates for such a study. Identifying distinct differences in circumstellar chemistry between these objects and the 21 μm sources could point to the pathways for the formation of the carrier of the 21 μm feature.

2.6 Conclusion

The 21 μm feature remains an enigma. Of the many proposed carriers all seem to have serious drawbacks. When originally discovered in the post-AGB objects it was hoped that the feature would be detected in other stages of the evolution of carbon stars, but to date evidence for any detection of the feature in either PNe or on the AGB has been tentative at best. In the future we may have the capability to re-observe the few carbon stars and PNe in which the *ISO* spectra suggested a weak 21 μm feature in order to either confirm or rule out the marginal detections. Any detection of the feature for stars outside the range of spectral classes from G to B would be important in understanding what is happening to the feature as the star evolves.

A number of attempts have been made to observe the resolved dust shells of these sources at different wavelengths and thereby demonstrate a separation of the 21 μm emission from that of the general continuum. None of these ground-based observations have shown any separation of emission components. It may be that space-based observations are needed to get the angular resolution and sensitivity required for this task. If the features cannot be separated, then the 21 μm carrier must be very closely related to the bulk grains in the dust shell, which are generally thought to be amorphous carbon grains. The transience of the feature suggests that one should be able to detect a difference between images obtained at 20 μm and adjacent wavelengths off of the feature. One would need to make such observations for a number of wavelengths and for objects with different contrasts between the 21 μm feature and the adjacent features to be able to draw any conclusions about the carriers. It may be that the angular scale of the variations is simply much smaller than can be probed with ground-based telescopes, unless interferometry or other high-resolution imaging methods become available at these wavelengths.

The post-AGB phase of evolution is short by stellar standards, if still long by human standards. If some of these 21 μm objects are found to be of relatively high luminosity and hence evolve faster than average, then even over a few decades we may observe some evolution of the central stars and their envelopes. Future mid-infrared observations of these objects and related types of stars may eventually detect changes that shed light on the formation and evolution of the 21 μm feature.

Three decades of study of the 21 μm feature have yielded a number of fascinating clues about the nature of its carrier, and while we have many hypotheses, we still lack a good identification. Better observational methods, using instruments with better spectral resolving power, sensitivity, and angular resolution are coming. They may help solve this enduring puzzle.

Acknowledgements This work has made use of data from the European Space Agency (ESA) mission *Gaia* (https://www.cosmos.esa.int/gaia), processed by the *Gaia* Data Processing and Analysis Consortium (DPAC, https://www.cosmos.esa.int/web/gaia/dpac/consortium). Funding for the DPAC has been provided by national institutions, in particular the institutions participating in the *Gaia* Multilateral Agreement.

This research has made use of the NASA/IPAC Infrared Science Archive, which is operated by the Jet Propulsion Laboratory, California Institute of Technology, under contract with the National Aeronautics and Space Administration.

This research has also made use of the NASA Astrophysics Data System, the SIMBAD and VizieR services of the Centre de Donnees astronomiques de Strasbourg, and the Pan-STARRS survey.

Conflict of Interest The authors declare that they have no conflict of interest.

References

Abia, C., Isern, J.: Astrophys. J. **536**, 438 (2000)
Abia, C., Cristallo, S., Cunha, K., de Laverny, P., Smith, V.V.: Astron. Astrophys. **625**, 40 (2019)
Alexander, C.M.O.D.: EAS Publ. Ser. **35**, 75–102 (2009)
Allamandolla, L.J., Tielens, A.G.G.M., Barker, J.R.: Astrophys. J. **290**, L25 (1985)
Allamandolla, L.J., Tielens, A.G.G.M., Barker, J.R.: Astrophys. J. Suppl. Ser. **71**, 733 (1989)
Bernard-Salas, J., Peeters, E., Sloan, G.C., Gutenkunst, S., Matsuura, M., Tielens, A.G.G.M., Zijlstra, A.A., Houck, J.R.: Astrophys. J. **699**, 1541 (2009)
Bernatowicz, T.J., Akande, O.W., Croat, T.K., Cowsik, R.: Astrophys. J. **631**, 988 (2005)
Bond, H.E., Ciardullo, R., Siegel, M.H.: Astron. J. **151**, 40 (2016)
Brown, A.G.A., Vallenari, A., Prusti, T., de Bruijne, J.H.J., et al.: Astron. Astrophys. **616**, 1 (2018)
Buss, R.H. Jr., Cohen, M., Tielens, A.G.G.M., Werner, M.W., Bregman, J.D., Witteborn, F.C., Rank, D., Sandford, S.A.: Astrophys. J. **365**, 23 (1990)
Buss, R.H. Jr., Tielens, A.G.G.M., Cohen, M., Werner, M.W., Bregman, J.D., Witteborn, F.C.: Astrophys. J. **415**, 250 (1993)
Cami, J., Bernard-Salas, J., Peeters, E., Malek, S.E.: Science **329**, 1850 (2010)
Cami, J., Sloan, G.C., Markwick-Kemper, A.J., Zijlstra, A.A., Bauschlicher, C.W. Jr., et al.: Astrophys. J. **690**, L122 (2009)
Cerrigone, L., Hora, J.L., Umana, G., Trigilio, C., Hart, A., Fazio, G.: Astrophys. J. **738**, 121 (2011)
Chang, H.-C.: J. Phys. Conf. Ser. **728**(6), 062004 (2016)
Chen, P.S., Shan, H.G.: Astron. J. **144**, 10 (2012)
Clément, D., Mutschke, H., Klein, R., Jäger, C., Dorschner, J., Sturm, E., Henning, Th.: Astrophys. J. **594**, 642 (2005)

Chigai, T., Yamamoto, T., Kaito, C., Kimura, Y.: Astrophys. J. **587**, 771 (2003)
Cox, P.: Astron. Astrophys. **236**, L29 (1990)
Cox, A.N.: Allen's Astrophysical Quantities (4th edition) ed. by A.N. Cox Springer, New York (2000)
Danilovich, T., Ramstedt, S., Gobrecht, D., Decin, L., De Beck, E., Olofsson, H.: Astron. Astrophys. **617**, 132 (2018)
Decin, L., Van Winckel, H., Waelkins, C., Bakker, E.J.: Astron. Astrophys. **332**, 928 (1998)
Decin, L., Agúndez, M., Barlow, M.J., Daniel, F., Cernicharo, J., Lombaert, R., et al.: Nature **467**, 7311 (2010)
De Smedt, K., Van Winckel, H., Karakas, A.I., Siess, L., Goriely, S., Wood, P.R.: Astron. Astrophys. **541**, 67 (2012)
De Smedt, K., Van Winckel, H., Kamath, D., Siess, L., Goriely, S., Karakas, A.I., Manick, R.: Astron. Astrophys. **587**, 6 (2016)
Evans, D.W., Riello, M., De Angeli, F., et al.: Astron. Astrophys. **616**, 4 (2018)
Forrest, W.J., Houck, J.R., McCarthy, J.F.: Astrophys. J. **248**, 195 (1981)
Geballe, T.R., Tielens, A.G.G.M., Kwok, S., Hrivnak, B.J.: Astrophys. J. **387**, 89 (1992)
Geballe, T.R., van der Veen, W.E.C.J.: Astron. Astrophys. **235**, L9 (1990)
Gillett, F.C., Forrest, W.J., Merrill, K.M.: Astrophys. J. **183**, 87 (1973)
Giridhar, S., Ferro, A.A.: Astron. Astrophys. **443**, 297 (2005)
Gladkowski, M., Szczerba, R., Sloan, G.C., Lagadec, E., Volk, K.: Astron. Astrophys. **626**, 92 (2019)
Garcia-Lario, P., Manchado, A., Ulla, A., Manteiga, M.: Astrophys. J. **513**, 941 (1999)
Goebel, J.H., Moseley, S.H.: Astrophys. J. **290**, 35 (1985)
Goebel, J.H.: Astron. Astrophys. **278**, 226 (1993)
Gómez-Llanos, V., Morisset, C., Szczerba, R., Garcia-Herández, D.A., Garcia-Lario, P.: Astron. Astrophys. **617**, 85 (2018)
Gonneau, A., Lancon, A., Trager, S.C., Aringer, B., Nowotny, W., Peletier, R.F., Prugniel, P., Chen, Y.-P., Lyubenova, M.: Astron. Astrophys. **601**, 141 (2017)
Goto, M., Gaessler, W., Hayano, Y., Iye, M., Kamata, Y., et al.: Astrophys. J. **589**, 419 (2003)
Grasdalen, G.L., Joyce, R.R.: Astrophys. J. **205**, L11 (1976)
Grishko, V.I., Tereschuk, K., Duley, W.W., Bernath, P.: Astrophys. J. **558**, 129 (2001)
Groenewegen, M.A.T., Wood, P.R., Sloan, G.C., et al.: Mon. Not. R. Astron. Soc. **376**, 313 (2007)
Gruendl, R.A., Chu, Y.-H., Seale, J.P., Matsuura, M., Speck, A.K., Sloan, G.C., Looney, L.W.: Astrophys. J. **688**, L9 (2008)
Haenecour, P., Floss, C., José, J., Amari, S., Lodders, K., Jadhav, M., Wang, A., Gyngard, F.: Astrophys. J. **825**, 88 (2016)
Hankins, M.J., Herter, T.L., Maercker, M., Lau, R.M., Sloan, G.C.: Astrophys. J. **852**, 27 (2018)
Hill, H.G.M., Jones, A.P., D'Hendecourt, L.B.: Astron. Astrophys. **336**, L41 (1998)
Hony, S., Waters, L.B.F.M., Tielens, A.G.G.M.: Astron. Astrophys. **390**, 533 (2002)
Hony, S., Tielens, A.G.G.M., Waters, L.B.F.M., de Koter, A.: Astron. Astrophys. **402**, 211 (2003)
Hony, S., Heras, A.M., Molster, F.J., Smolders, K.: Astron. Astrophys. **501**, 609 (2009)
Hrivnak, B.J., Volk, K., Kwok, S.: Astrophys. J. **535**, 275 (2000)
Hrivnak, B.J., Volk, K., Kwok, S.: Astrophys. J. **694**, 1147 (2009)
Hrivnak, B.J.: Astrophys. J. **438**, 341 (1995)
Hrivnak, B.J., Kwok, S.: Astrophys. J. **513**, 869 (1999)
Hrivnak, B.J., Lu, W., Volk, K., Szczerba, R., Soszynski, I., Hajduk, M.: Astrophys. J. **805**, 78 (2015)
Hrivnak, B.J., Van de Steene, G., Van Winckel, H., Sperauskas, J., Bohlender, D., Lu, W.: Astrophys. J. **846**, 96 (2017)
Jones, A.P., Duley, W.W., Williams, D.A.: Q. J. R. Astron. Soc. **31**, 567 (1990)
Justtanont, K., Barlow, M.J., Skinner, C.J., Roche, P.F., Aitken, D.K., Smith, C.H.: Astron. Astrophys. **309**, 612 (1996)
Kessler, M.F., Steinz, J.A., Anderegg, M.E., Clavel, J., Drechsel, G., et al.: Astron. Astrophys. **315**, L27 (1996)
Kimura, Y., Nuth, J.A., Ferguson, F.T.: Meteoritics **41**, 673 (2005)
Klochkova, V.G., Szczerba, R., Panchuk, V.E., Volk, K.: Astron. Astrophys. **345**, 905 (1999)
Klochkova, V.G., Ushkin, M.V., Miroshnichenko, A.S., Panchuk, V.E., Bjorkman, K.S.: (2002)
Kraus, G.F., Nuth, J.A., Nelson, R.N.: Astron. Astrophys. **328**, 419 (1997)
Kraemer, K.E., Sloan, G.C., Price, S.D., Walker, H.J.: Astrophys. J. Suppl. Ser. **140**, 389 (2002)
Kwok, S., Volk, K., Bernath, P.: Astrophys. J. **554**, L87 (2001)
Kwok, S., Volk, K., Hrivnak, B.J.: Astrophys. J. **345**, L51 (1989)
Kwok, S., Volk, K., Hrivnak, B.J.: Astrophys. J. **573**, 720 (2002)
Kwok, S., Zhang, Y.: Astrophys. J. **771**, 5 (2013)
Lagadec, E., Verhoelst, T., Mékarnia, D., Suáeez, O., Zijlstra, A.A., Bendjoya, P., et al.: Mon. Not. R. Astron. Soc. **417**, 32 (2011)
Lagadec, E., Sloan, G.C., Zijlstra, A., Mauron, N., Houck, J.R.: Mon. Not. R. Astron. Soc. **427**, 2588 (2012)
Lau, R.M., Werner, M., Sahai, R., Ressler, M.E.: Astrophys. J. **833**, 115 (2016)
Leger, A., Puget, J.L.: Astron. Astrophys. **137**, L5 (1984)
Leisenring, J.M., Kemper, F., Sloan, G.C.: Astrophys. J. **681**, 1557 (2008)
Li, A., Draine, B.T.: Astrophys. J. **554**, 778 (2001)
Li, A.: Astrophys. J. **599**, L45 (2003)
Lindegren, L., Hernández, J., Bombrun, A., Klioner, S., et al.: Astron. Astrophys. **616**, 2 (2018)
Lombaert, R., de Vries, B.L., de Koter, A., Decin, L., Min, M., Smolders, K., Mutschke, H., Waters, L.B.F.M.: Astron. Astrophys. **544**, 18 (2012)
Maercker, M., Mohamed, S., Vlemmings, W.H.T., Ramstedt, S., Groenewegen, M.A.T., et al.: Nature **490**, 232 (2012)
Martin, P.G., Rogers, C.: Astrophys. J. **322**, 374 (1987)
Matsuura, M., Bernard-Salas, J., Lloyd Evans, T., Volk, K., et al.: Mon. Not. R. Astron. Soc. **439**, 1472 (2014)
McCuskey, S.W.: Astrophys. J. Suppl. Ser. **2**, 75 (1955)
Meixner, M., Skinner, C.J., Graham, J.R., Keto, E., Jernigan, J.G., Arens, J.F.: Astrophys. J. **482**, 897 (1997)
Meixner, M., Zalucha, A., Ueta, T., Fong, D., Justtanont, K.: Astrophys. J. **614**, 731 (2004)
Messenger, S.J., Speck, A., Volk, K.: Astrophys. J. **764**, 142 (2013)
Mishra, A., Li, A., Jiang, B.W.: Astrophys. J. **802**, 39 (2015)
Mishra, A., Li, A., Jiang, B.W.: Astrophys. J. **825**, 68 (2016)
Neufeld, D.A., González-Alfonso, E., Melnick, G., Szczerba, R., et al.: Astrophys. J. **272**, L29 (2011)
Nuth, J.A., Moseley, S.H., Silverberg, R.F., Geobel, J.H., Moore, W.J.: Astrophys. J. **290**, 41 (1985)
Olnon, F.M., Raimond, E., Neugebauer, G., van Duinen, R.J., Habing, H.J., et al.: Astron. Astrophys. Suppl. Ser. **65**, 607 (1986)
Omont, A., Moseley, S.H., Cox, P., Glaccum, W., Casey, S., Forveille, T., Chan, K.-W., Szczerba, R., Loewenstein, R.F., Harvey, P.M., Kwok, S.: Astrophys. J. **454**, 819 (1995)
Paradis, D., Reach, W.T., Bernard, J.-Ph., et al.: Astrophys. J. **138**, 196 (2009)
Papoular, R., Conrad, J., Giuliano, M., Kister, J., Mille, G.: Astron. Astrophys. **214**, 204 (1989)
Papoular, R.: Astron. Astrophys. **362**, L9 (2000)
Papoular, R.: Mon. Not. R. Astron. Soc. **415**, 494 (2011)
Pei, A., Volk, K.: In: Kwok, S., Dopita, M., Sutherland, R. (eds.) I.A.U. Symposium 209, Planetary Nebulae: Their Evolution and Role in the Universe. PASP, San Francisco, CA (2003)
Peeters, E.H., Van Kerckhoven, C., Tielens, A.G.G.M., Allamondola, L.J., Hudgins, D.M., Bauschlicher, C.W.: Astron. Astrophys. **390**, 1089 (2002)

Pino, T., Dartois, E., Cao, A.-T., Carpentier, Y., Chamaillé, et al.: Astron. Astrophys. **490**, 665 (2008)
Posch, Th., Mutschke, H., Anderson, A.: Astrophys. J. **616**, 1167 (2004)
Raman, V.V., Anandarao, B.G., Janardhan, P., Pandey, R.: Mon. Not. R. Astron. Soc. **470**, 1593 (2017)
Reddy, B.E., Bakker, E.J., Hrivnak, B.J.: Astrophys. J. **524**, 831 (1999)
Reddy, B.E., Lambert, D.L., Gonzalez, G., Yong, D.: Astrophys. J. **564**, 482 (2002)
Rho, J., Kozasa, T., Reach, W.T., Smith, J.D., Rudnick, L., DeLaney, T., Ennis, J.A., Gomez, H., Tappe, A.: Astrophys. J. **673**, 271 (2008)
Rho, J., Gomez, H.L., Boogert, A., Smith, M.W.L., Lagage, P.-O., et al.: Mon. Not. R. Astron. Soc. **479**, 510 (2018)
Richter, M.J., Dewitt, C.N., McKelvey, M., Montiel, E., McMurray, R., Case, M.E.: J. Astron. Instrum. **7**, 13 (2018)
Rouleau, F., Martin, P.G.: Astrophys. J. **377**, 526 (1991)
Sánchez Contreras, C., Sahai, R., Gil de Paz, A., Goodrich, R.: Astrophys. J. Suppl. Ser. **179**, 166 (2008)
Sellgren, K.: Astrophys. J. **277**, 623 (1984)
Sloan, G.C., Hony, S., Smolders, K., Decin, L., Ziljstra, A.A., et al.: Astrophys. J. **729**, 121 (2011)
Sloan, G.C., Kraemer, K.E., Matsuura, M., Wood, P.R., Price, S.D., Egan, M.P.: Astrophys. J. **645**, 1118 (2006)
Sloan, G.C., Herter, T.L., Charmandaris, V., Sheth, K., Burgdorf, M., et al.: Astron. J. **149**, 11 (2015)
Sloan, G.C., Jura, M., Duley, W.W., Kraemer, K.E., Bernard-Salas, J., et al.: Astrophys. J. **664**, 1144 (2007)
Sloan, G.C., Lagadec, E., Zijlstra, A.A., Kraemer, K.E., Weis, A.P., et al.: Astrophys. J. **791**, 28 (2014)
Smolders, K., Neyskens, P., Blommaert, J.A.D.L., Hony, S., van Winckel, H., et al.: Astron. Astrophys. **540**, 72 (2012)
Sourisseau, C., Coddens, G., Papoular, R.: Astron. Astrophys. **254**, L1 (1992)
Speck, A.K., Hofmeister, A.M.: Astrophys. J. **600**, 986 (2004)
Suárez, O., García-Lario, P., Manchado, A., Manteiga, M., Ulla, A., Pottasch, S.R.: Astron. Astrophys. **458**, 173 (2006)
Szczerba, R., Henning, Th., Volk, K., Kwok, S., Cox, P.: Astron. Astrophys. **345**, 39 (1999)
Tielens, A.G.G.M.: Annu. Rev. Astron. Astrophys. **46**, 289 (2008)
Tokunaga, A.L., Young, E.T.: Astrophys. J. **237**, L93 (1980)
van Aarle, E., van Winckel, H., de Smedt, K., Karnath, D., Wood, P.R.: Astron. Astrophys. **554**, 106 (2013)
Van Winckel, H., Reyniers, M.: Astron. Astrophys. **354**, 135 (2000)
Vickers, S.B., Frew, D.J., Parker, Q.A., Bojičić, I.S.: Mon. Not. R. Astron. Soc. **447**, 1673 (2015)
Volk, K., Kwok, S., Hrivnak, B.J.: Astrophys. J. **516**, 99 (1999)
Volk, K., Kwok, S., Stencel, R.E., Brugel, E.: Astrophys. J. Suppl. Ser. **77**, 607 (1991)
Volk, K., Xiong, G.-Z., Kwok, S.: Astrophys. J. **503**, 408 (2000)
Volk, K., Kwok, S., Hrivnak, B.J., Szczerba, R.: Astrophys. J. **567**, 41 (2002)
Volk, K., Hrivnak, B.J., Matsuura, M., Bernard-Salas, J., Szczerba, R., et al.: Astrophys. J. **735**, 127 (2011)
von Helden, G., Tielens, A.G.G.M., van Heijnsbergen, D., Duncan, M.A., Hony, S., Waters, L.B.F.M., Meijer, G.: Science **288**, 313 (2000)
Werner, M.W., Roellig, T.L., Low, F.J., Rieke, G.H., Rieke, M., et al.: Astrophys. J. Suppl. Ser. **154**, 1 (2004)
Webster, A.: Mon. Not. R. Astron. Soc. **277**, 1555 (1995)
Wells, M., Pel, J.-W., Glasse, A., Wright, G.S., Aitink-Kroes, G., et al.: Publ. Astron. Soc. Pac. **127**, 646 (2015)
Wright, E.L., Eisenhardt, P.R.M., Mainzer, A.K., Ressler, M.E., Cutri, R.M., et al.: Astron. J. **140**, 1868 (2010)
Zacs, L., Klochkova, V.G., Panchuk, V.E.: Mon. Not. R. Astron. Soc. **275**, 764 (1995)
Zhang, K., Jiang, B.W., Li, A.: Astrophys. J. **702**, 680 (2009)
Zhukovska, S., Gail, H.P.: Astron. Astrophys. **486**, 229 (2008)
Zubko, V.G., Mennella, V., Colangeli, L., Bussoletti, E.: Mon. Not. R. Astron. Soc. **282**, 321 (1996)